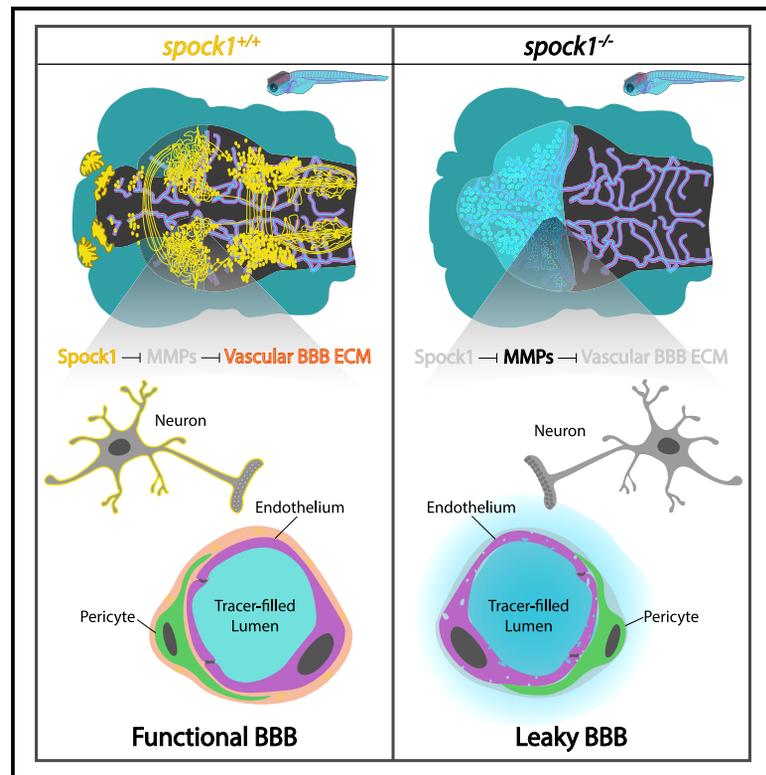# Developmental Cell

The secreted neuronal signal Spock1 promotes blood-brain barrier development

Graphical abstract

Authors

Natasha M. O'Brown, Nikit B. Patel, Ursula Hartmann, Allon M. Klein, Chenghua Gu, Sean G. Megason

Correspondence

natasha.obrown@rutgers.edu (N.M.O.), megason@hms.harvard.edu (S.G.M.)

In brief

The blood-brain barrier (BBB) restricts movement of solutes across brain blood vessels, and understanding BBB formation will help drug delivery and treatment of neurodegenerative disease, where it often fails. Here, O'Brown et al. identify a secreted signal, Spock1, that is expressed in neurons and that induces BBB properties in surrounding brain vasculature.

Highlights

- Spock1, secreted from neurons, induces BBB functional development

- Spock1 regulates vascular basement membrane composition

- Exogenous SPOCK1 can partially restore BBB function in leaky mutants

CelPress

Developmental Cell

CellPress

Article

The secreted neuronal signal Spock1 promotes blood-brain barrier development

Natasha M. O'Brown,[1,4,*] Nikit B. Patel,[1] Ursula Hartmann,[2] Allon M. Klein,[1] Chenghua Gu,[3] and Sean G. Megason[1,*]
[1]Department of Systems Biology, Harvard Medical School, 200 Longwood Ave, Boston, MA 02115, USA
[2]Center for Biochemistry, Medical Faculty, University of Cologne, Joseph-Stelzmann-Str. 52, 50931 Cologne, Germany
[3]Howard Hughes Medical Institute, Department of Neurobiology, Harvard Medical School, 220 Longwood Ave, Boston, MA 02115, USA
[4]Lead contact
*Correspondence: natasha.obrown@rutgers.edu (N.M.O.), megason@hms.harvard.edu (S.G.M.)
https://doi.org/10.1016/j.devcel.2023.06.005

SUMMARY

The blood-brain barrier (BBB) is a unique set of properties of the brain vasculature which severely restrict its permeability to proteins and small molecules. Classic chick-quail chimera studies have shown that these properties are not intrinsic to the brain vasculature but rather are induced by surrounding neural tissue. Here, we identify Spock1 as a candidate neuronal signal for regulating BBB permeability in zebrafish and mice. Mosaic genetic analysis shows that neuronally expressed Spock1 is cell non-autonomously required for a functional BBB. Leakage in *spock1* mutants is associated with altered extracellular matrix (ECM), increased endothelial transcytosis, and altered pericyte-endothelial interactions. Furthermore, a single dose of recombinant SPOCK1 partially restores BBB function in *spock1* mutants by quenching gelatinase activity and restoring vascular expression of BBB genes including *mcamb*. These analyses support a model in which neuronally secreted Spock1 initiates BBB properties by altering the ECM, thereby regulating pericyte-endothelial interactions and downstream vascular gene expression.

INTRODUCTION

The blood-brain barrier (BBB) maintains a tightly controlled homeostatic environment in the brain that is required for proper neural function. BBB breakdown has been implicated in multiple neurodegenerative diseases including Alzheimer's, Parkinson's, and Huntington's diseases.[1] Conversely, the BBB also serves as an obstacle for effective drug delivery to the brain. Therefore, there is great interest in generating a better understanding of how to therapeutically regulate its permeability, both to restore BBB function in neurodegeneration and to transiently open it for improved chemotherapeutic access for brain tumors. The BBB is a specialized property of the brain vasculature, which is composed of a thin, continuous layer of non-fenestrated endothelial cells with uniquely restrictive properties. Brain endothelial cells create the barrier via two primary cellular mechanisms: (1) specialized tight junction complexes that block the transit of small water-soluble molecules between cells and (2) reduced levels of vesicular trafficking or transcytosis to restrict transit through endothelial cells.[2] At a molecular level, functional barrier endothelial cells are differentiated from peripheral endothelial cells by high expression of the tight junction molecule Claudin-5[3] and the fatty acid transporter Mfsd2a,[4,5] and an absence of the fenestra and vesicle-associated protein PLVAP.[6] Expression of substrate-specific influx and efflux transporters such as Glut1[7] and Pgp,[8] which dynamically regulate the intake of

necessary nutrients and the removal of metabolic waste products,[9] further enhances the selectivity of the BBB.

The restrictive properties of the BBB are not intrinsic to brain endothelial cells but are induced and maintained by signals in the brain microenvironment during embryonic development.[10] When avascularized quail neural tissue was transplanted into embryonic chicken gut cavities, the blood vessels ingressing from the non-barrier gut tissue obtained functional BBB properties, specifically both tight junctions and reduced levels of vesicles, resulting in trypan blue tracer confinement within the blood vessels.[10] Conversely, when avascularized quail somite tissue was transplanted into embryonic chick brain, the blood vessels ingressing from the neural tissue lost functional BBB properties, leaking tracer into the quail graft due to increased endothelial transcytosis and loss of tight junction function. These data show that signals from the neural microenvironment to the vasculature control barrier function. Furthermore, these microenvironmental signals are also required to actively maintain barrier properties throughout life.[11–14]

Mural cells called pericytes share the endothelial basement membrane and co-migrate with endothelial cells during neovascularization of the developing brain. This close interaction between pericytes and endothelial cells is required for both the initiation and continued maintenance of barrier properties.[15–17] Astrocytes, glial cells found exclusively in the central nervous system (CNS), completely ensheath the vasculature with their endfeet in a polarized fashion.[18] Astrocytes arise late in

embryonic development, after neurogenesis is complete, with the vast majority of gliogenesis occurring postnatally in rodents. Mammalian astrocytes are potent inducers of barrier properties *in vitro* and *in vivo* and are required for BBB maintenance.[13,14,19] While the necessity of these two cell types has been known for decades, canonical Wnt signaling arising from both neuronal and astrocytic sources is the only microenvironmental signal known to induce and maintain BBB function.[13,20–27] However, in addition to its role in regulating barrier properties, Wnt signaling also plays an important role in tip cell specification and angiogenesis in the developing brain.[21,23,24] Furthermore, mouse endothelial cells are Wnt responsive as early as embryonic day (E) 9.5,[27] preceding the acquisition of functional barrier properties,[22] suggesting that other signaling may be acting in conjunction with or in addition to Wnt signaling for the induction of BBB properties.

To further examine the molecular determinants of BBB development, we turned to the optically transparent zebrafish system, which allows for imaging of the intact BBB *in toto* throughout zebrafish development. Zebrafish brain endothelial cells express many of the same molecular markers as mammalian brain endothelial cells, including Glut1, Cldn5, ZO-1, and Mfsd2a.[24,28–32] We previously characterized the molecular and subcellular mechanisms of functional BBB development in zebrafish and determined that the zebrafish BBB becomes functionally mature by 5 days post fertilization (dpf) due to the suppression of transcytosis rather than through the acquisition of tight junction function, which was observed as early as 3 dpf.[28] During these studies, we serendipitously discovered a recessive viable mutant with profound forebrain and midbrain barrier leakage, which we identify here to be the neuronally produced and secreted proteoglycan Spock1. Using an array of perturbations and imaging techniques, we uncover the range of Spock1 signaling to the vasculature and identify that mechanistically, Spock1 signaling acts through control of the pericyte-endothelial extracellular matrix (ECM) to control endothelial transcytosis.

RESULTS

Identification and mapping of a spontaneous leaky mutant to *spock1*

We found a spontaneous recessive mutant that leaks both an injected 1 kDa Alexa Fluor (AF) 405 NHS ester dye and a transgenic 80-kDa serum vitamin D binding protein (DBP)-EGFP[29] into the forebrain and midbrain as early as 3 dpf with no improvement in BBB function throughout larval development (Figures 1A–1E) or adulthood (Figure 1G). This increased BBB permeability in homozygous mutants occurs in the absence of hemorrhage or vascular patterning defects (Figure S1), apparent changes in Wnt signaling (Figure S1), or any reduction in viability or fertility. Time-lapse imaging of injected 10-kDa Dextran revealed a steady accumulation of Dextran in the brain parenchyma of leaky mutants over the course of 1 h (Figure S2). The rate of Dextran accumulation in the brain closely resembled the dynamics of Dextran leakage we previously reported in *mfsd2aa* mutants,[28] which specifically display an increase in endothelial caveolae-mediated transcytosis without altered tight junction function.

To identify the mutation responsible for this leakage phenotype, we performed linkage mapping on 5 dpf mutant and wild type siblings using bulk segregant RNA-seq[33] and identified a single peak at chr14:2205271-3513919 (GRCz11; Figures 1H and S3). Of the 14 genes within the linkage region (Figure S3), 8 were expressed at 5 dpf. Two of these genes were differentially expressed between mutant and wild type, *csf1ra*, and *gstp2* (Table S1), and one had several mutations that segregated with the leakage phenotype, *spock1*. To test whether loss of any of these genes conferred the increased BBB permeability, we assessed tracer leakage in mosaic crispants (zebrafish larvae injected at the 1-cell stage with Cas9 protein and gene-specific sgRNAs) at 5 dpf and observed no BBB defects in 42 *gstp2* or 35 *csf1ra* crispants. However, when we assessed BBB function in *spock1* crispants, we observed a strong leaky phenotype in 26% of larvae (26/100 injected fish; Figure S3) and moderate leakage in 53% (53/100 injected fish; Figure S3) as well as a few that displayed BBB leakage restricted to one midbrain hemisphere (4/100 injected fish; Figure S3). Leakage in *spock1* crispants corresponded with a loss of *spock1* expression (Figure S3). *Spock1* encodes a secreted protein of unclear function named for its conserved protein domains: SPARC (Osteonectin), Cwcv and kazal-like domains proteoglycan 1 protein (also known as Testican-1). Spock1 has three predicted domains: (1) a kazal-type serine protease inhibitor, (2) an extracellular SPARC calcium-binding region, and (3) a thyroglobulin type-1 repeat region, in addition to being decorated by both chondroitin sulfate (CS) and heparan sulfate (HS) glycosaminoglycan (GAG) chains (Figure 1I).[34,35] Further sequencing of *spock1* confirmed a few point mutations in the SPARC calcium-binding domain in the leaky fish (Figure 1I), including a T241A missense mutation and two silent mutations at Q249 and G250, hereafter referred to as *spock1*[hm41/hm41] mutants.

To validate that loss of Spock1 function causes the leakage phenotype in the spontaneous mutants, we generated a stable null allele designated *spock1*[hm43] using CRISPR mutagenesis with two sgRNAs to completely delete the 5′ UTR and start codon of *spock1* (Figure 1I). As expected, based on the 550-bp genomic deletion, *spock1*[hm43/hm43] fish do not transcribe *spock1* unlike the original spontaneous *spock1*[hm41/hm41] mutants, which maintain normal *spock1* transcription (Figure S4). Functional tracer leakage assays using 10-kDa Dextran revealed the same increased BBB permeability specifically in the forebrain and the midbrain observed in the spontaneous *spock1*[hm41/hm41] mutants (Figures 1J–1L). This increased BBB permeability was accompanied with increased expression of the pathological marker of leaky endothelial cells *plvapb:EGFP*[31] compared with the negligible levels observed in wild type siblings with a functional BBB (Figures 1M–1O). Lastly, we crossed both lines to test for genetic complementation and observed the leaky phenotype in *spock1*[hm41/hm43] compound heterozygotes (Figures 1P–1S), further indicating that the initial spontaneous mutant acts via loss of Spock1 function.

Neuronal Spock1 signals to the vasculature within a short range

Given the necessity of Spock1 in determining BBB function, we next wanted to assess where *spock1* was expressed
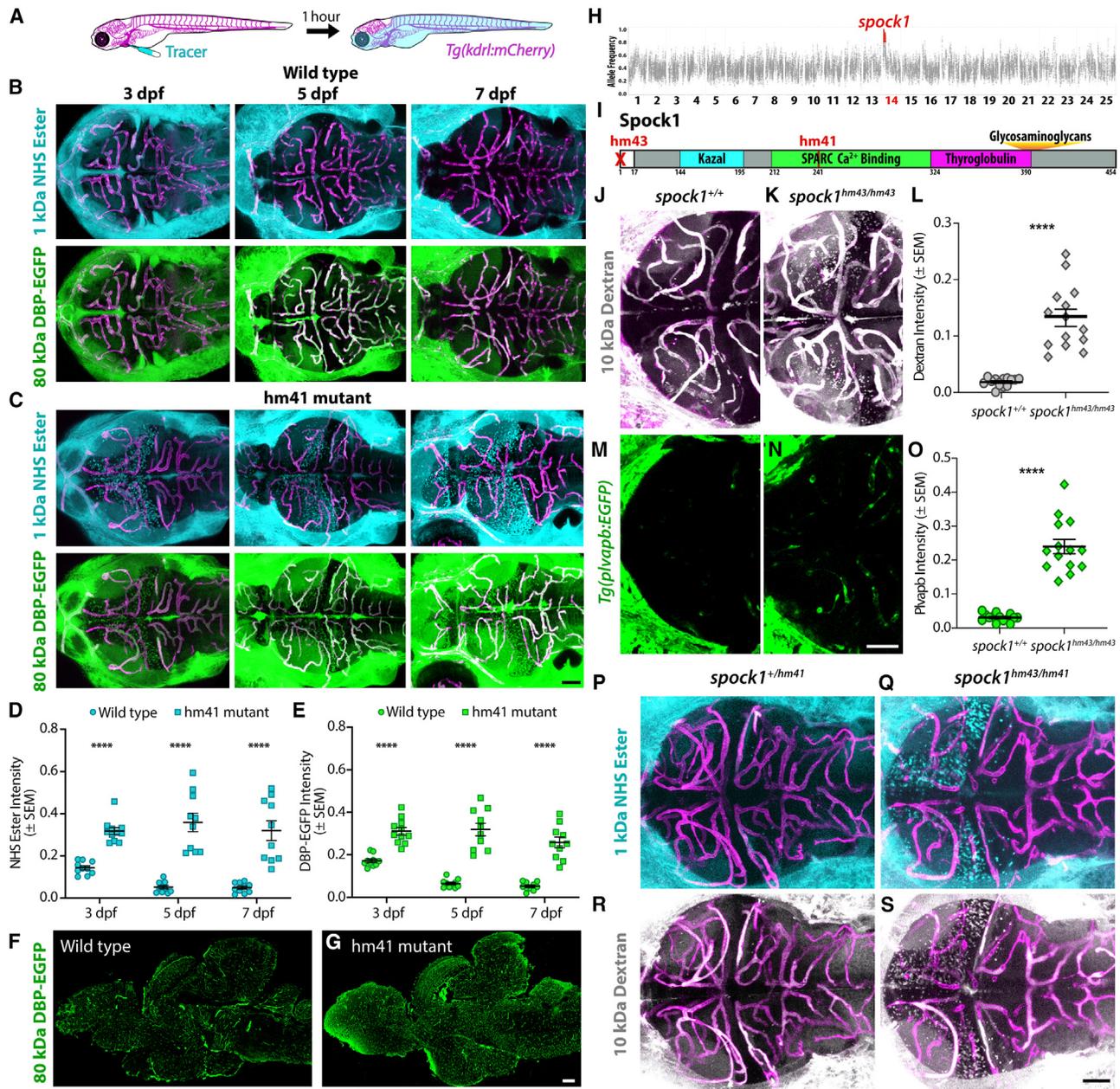
Developmental Cell
Article

CellPress

Figure 1. Spock1 induces BBB functional development

(A–E) Fluorescent tracer leakage assays in larval zebrafish reveal BBB leakage in the forebrain and midbrain of both injected 1-kDa Alexa Fluor 405 NHS Ester (turquoise) and 80 kDa DBP-EGFP (green) of *hm41* homozygous larvae (C) compared with wild type controls (B) throughout larval development, as quantified in (D) and (E).

(F and G) Sagittal sections of adult brains show that the mutant leakage persists into adulthood (G).
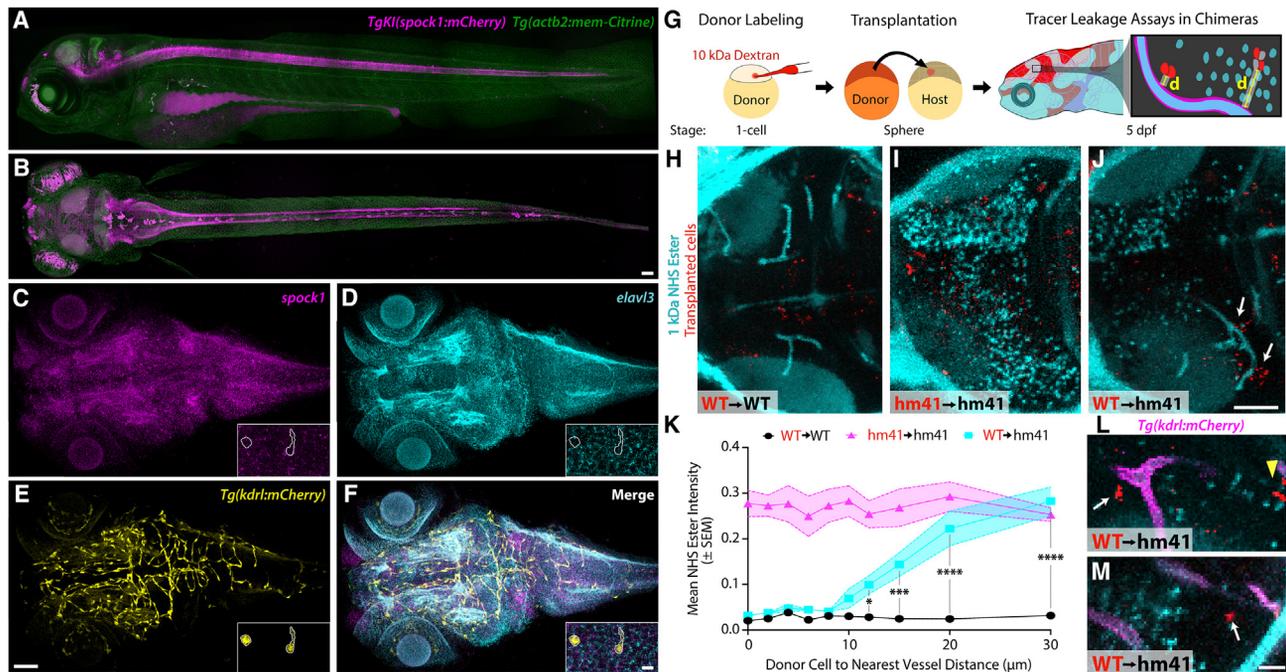
(H) Linkage mapping of the *hm41* mutant phenotype reveals tight linkage to *spock1* on chromosome 14.

(I) *Spock1hm41* has several point mutations (T241A and several silent mutations) in the SPARC domain. *Spock1hm43* has a deletion of the 5′ UTR and start codon.

(J–O) Dextran leakage assays show *spock1hm43/hm43* mutants (K) have increased BBB leakage (L). *spock1hm43/hm43* mutants also have increased expression of the leaky vessel marker *plvapb* (N and O).

(P–S) Compound *spock1hm43/hm41* heterozygotes also display increased NHS Ester (Q) and Dextran (S) leakage compared with *spock1hm41/+* heterozygote siblings, which confine both injected tracers at 5 dpf (P and R). Scale bars represent 50 μm (C, N, and S) and 200 μm (G). n = 10 (D and E) and 14 (L and O), with each point representing an individual fish. ****p < 0.0001 by two-way ANOVA (D and E) and by t test (L and O).

during BBB development. Using CRISPR, we generated a stable *spock1* knock in mCherry reporter (*TgKI(spock1:mCherry)hm44*), which revealed expression throughout the developing

CNS, including the brain, retina, and spinal cord (Figures 2A, 2B, and S5). We validated *spock1* expression in the brain by whole-mount HCR fluorescent *in situ* hybridization (FISH)

Figure 2. Neuronal Spock1 regulates endothelial cells within a 10–20 μm range

(A and B) Sagittal (A) and dorsal (B) maximum intensity projections (MIPs) of the *TgKI(spock1:mCherry)* (magenta) knockin reveals expression of *spock1* throughout the CNS, including the retina, brain, and spinal cord with all cells in the fish labeled by Tg(*actb2:memCitrine*) (green).

(C–F) Whole-mount HCR *in situ* hybridization for *spock1* (C) confirms signal throughout the 5 dpf brain, in *elavl3*+ (D) neurons and absent from *kdrl*+ vasculature (E). Insets are zoomed in 10-μm thick MIPs from the midbrain region to further resolve the absence of *spock1* signal in the vasculature (outlined in white).

(G) Schematic of transplantation experiments. Cells from donor embryos labeled with 10-kDa dextran (red) at the single-cell stage are transplanted into unlabeled host embryos at sphere stage. Leakage of the injected 1-kDa AF 405 NHS Ester (turquoise) into the midbrain parenchyma is then measured in relationship to the distance (d) from the blood vessel to the nearest donor cell in the 5 dpf chimeric larvae.

(H–J) Representative dorsal 20-μm thick MIP confocal image of a chimeric larva with transplanted wild type donor cells (red) into a wild type host (H, WT → WT), *spock1*^{hm41/hm41} donor cells into a *spock1*^{hm41/hm41} mutant host (I, hm41 → hm41), and wild type donor cells into a *spock1*^{hm41/hm41} mutant host (J, WT → hm41).

(K) Quantification of mean NHS leakage in WT → WT (black line, n = 11) and hm41 → hm41 (magenta line, n = 8) reveals no change in tracer leakage in relationship to the nearest donor cell, with wild type fish confining the tracer and mutant fish leaking the tracer. However, WT → hm41 (turquoise line, n = 11) transplants reveal a full rescue of the leakage in the mutant background when the transplanted cell is within 10 μm of a blood vessel and no effect if the donor cell is further than 20 μm from the vessel.

(L–M) Zoomed in images of WT → hm41 transplants. The white arrows point to instances of local rescue of tracer (turquoise) leakage when the wild-type donor cell is close but not directly contacting the mutant vasculature (magenta). The yellow arrowhead marks wild-type donor cells that fall outside the range of Spock1 signaling. Scale bars represent 50 μm (D and K) and 10 μm (G and N). *p = 0.0495, ***p = 0.0001, ****p < 0.0001 by two-way ANOVA compared with WT → WT transplants.

and saw that it colocalized with the neuronal marker *elavl3* and never the vascular Tg(*kdrl:mCherry*) signal (Figures 2C–2F and S5), similar to its predominantly neural expression in the developing mouse CNS.[36] This neuronal expression was confirmed further in live double transgenic *TgKI(spock1:mCherry)* and *Tg(huc:GcAMP6s)* animals (Figure S5).[36] To determine whether *spock1* is expressed by a particular subtype of neuron, we co-stained for *spock1* and the glutamatergic marker *slc17a6b* and the GABAergic marker *gad1b* (Figure S5). These analyses revealed that while not every *elavl3*+ neuron expresses *spock1*, *spock1* expression was not restricted to either neuronal subtype. However, *spock1* expression did appear to be excluded from *Tg(neurog1:egfp)* neurons, indicating that *spock1* is primarily expressed by post-mitotic neurons (Figure S5). Prior single-cell RNA sequencing (scRNA-seq) data[37] and our own also showed expression of *spock1* primarily in neurons and never in vascular endothelial cells (Figure S6). Taken together, these data indicate that we have

identified a neuronal signal, Spock1, that plays a role in establishing endothelial BBB properties during development without altering vascular patterning.

To determine the range of the Spock1 signal, we performed cell transplantation experiments to make genetically mosaic zebrafish embryos and assessed tracer leakage in relationship to the closest transplanted cells at 5 dpf (Figure 2G). When we transplanted labeled wild type cells into wild type host embryos, we observed a negligible level of tracer accumulation in the brain parenchyma regardless of the proximity of the nearest donor cell (Figures 2H and 2K). In contrast, when we transplanted *spock1*^{hm41/hm41} mutant cells into mutant host embryos, we observed high levels of tracer accumulation in the parenchyma regardless of the proximity of the nearest donor cell (Figures 2I and 2K). Strikingly, when we transplanted wild type cells into *spock1* mutant hosts, we observed a complete rescue of the mutant leakage if the wild type donor cell was within 10 μm of a blood vessel, and no rescue if the donor cell was
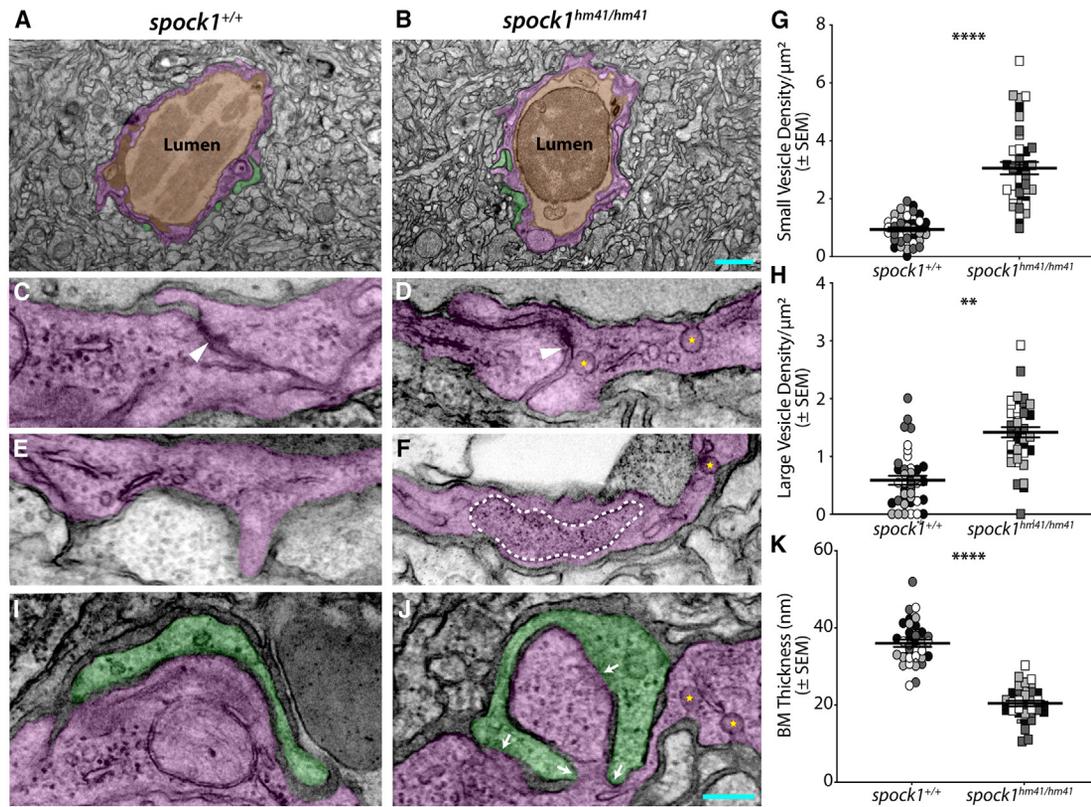
Developmental Cell
Article

CellPress

Figure 3. Spock1 mutant leakage arises through increased endothelial vesicles

(A and B) The neurovascular unit remains intact in *spock1hm41/hm41* mutants (B) with a continuous single layer of endothelial cells (pseudocolored magenta) enclosing the lumen (pseudocolored orange) and in close contact with pericytes (pseudocolored green).

(C–H) The majority of tight junctions (white arrowheads) are functionally restrictive in the *spock1hm41* mutant endothelial cells (88%). Mutant endothelial cells displayed a significant increase in vesicular density, including both small flask shaped vesicles (yellow stars, G) and larger vesicles greater than 200 nm in diameter (outlined by a white dashed line in F, H).

(I–K) While pericyte coverage is unaltered in *spock1hm41* mutants, the pericyte-endothelial cell interactions are altered in the mutants, with several instances of direct pericyte-endothelial cell contact (white arrows) and overall diminished average basement membrane (BM) thickness between the two vascular cells (K). Scale bars represent 1 μm (B) and 200 nm (J). n = 4 fish, each demarcated by a unique color, with 10 vessels analyzed per fish and shown as individual points. **p = 0.0029 (H), ****p < 0.0001 by nested t test (G and K).

more than 20 μm away (Figures 2J–2M), indicating that Spock1 can functionally signal at a distance of 10–20 μm. Importantly, wild type cells could rescue leakage in mutant hosts when they differentiate as neurons but not endothelial cells (Figure 2M).

Mutant leakage arises from increased transcytosis and altered pericyte-endothelial interactions

To assess the subcellular mechanism of increased BBB permeability in *spock1hm41/hm41* mutants, we injected electron-dense NHS-gold nanoparticles (5 nm) into circulation, followed by transmission electron microscopy (TEM) imaging in 7 dpf *spock1* mutant and wild type siblings. These TEM leakage assays revealed no alterations in the cellular composition of the neurovascular unit (NVU) in *spock1* mutants, with endothelial cells and pericytes sharing a basement membrane that is surrounded by glia and neurons (Figures 3A and 3B). A modest impairment in tight junction function was observed in *spock1* mutants (52/59 functional tight junctions; Figure 3D) compared with wild type siblings (57/57; Figure 3C). However, *spock1*

mutants had a significant increase in both small (<100 nm diameter) non-clathrin coated vesicles (Figures 3D and 3G) and large (>200 nm diameter) vesicles (Figures 3F and 3H) suggesting that the leakage results primarily from an increase in vesicular trafficking across endothelial cells. In addition to the increase in total large vesicular abundance in *spock1* mutants, we also observed several of these large vesicles fused to the abluminal membrane in multiple larvae with a few examples of the gold nanoparticles visibly spilling into the endothelial basement membrane (Figure 3F). Although pericyte coverage of the endothelium was unaltered (Figure S1), *spock1* mutants displayed overall thinner pericyte-endothelial basement membranes with several pericytes having long stretches of apparently direct contact on endothelial cells (Figures 3I–3K), corresponding with observations by live confocal microscopy (Figure S1). These data suggest that loss of Spock1 function alters the critical pericyte extracellular interactions with endothelial cells, resulting in loss of BBB properties as observed in pericyte-deficient mice and zebrafish.[16,17,38,39]
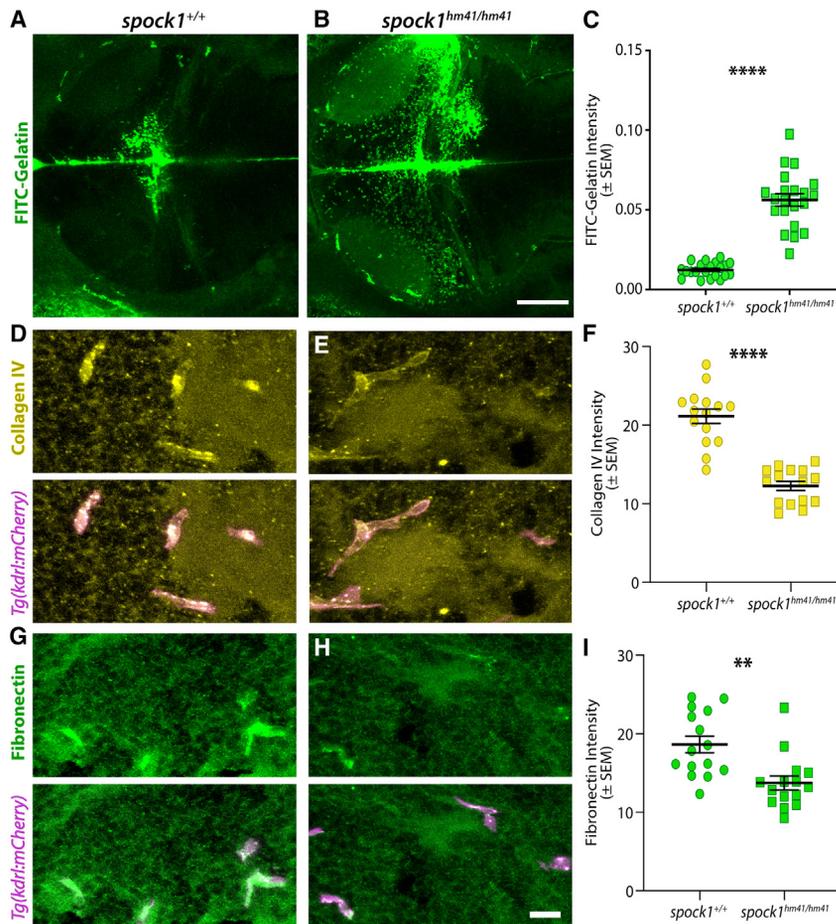
Figure 4. The extracellular matrix is misregulated in *spock1* mutants

(A–C) *In vivo* gelatin zymography in wild type (A) and *spock1*[hm41/hm41] mutants (B) reveals significantly increased gelatinase activity in the mutant midbrain compared with wild-type siblings (C).

(D–I) Immunofluorescence staining for vascular extracellular matrix proteins collagen IV (yellow, D–F) and fibronectin (green, G–I) that are required for vascular integrity reveal significantly reduced levels of all basement membrane proteins assayed within in the kdrl:mCherry labeled vasculature (magenta), quantified in (F) and (I). n = 21 (C) and 15 (F and I) fish analyzed for each genotype and depicted as individual points.

Scale bars represent 50 μm (B) and 10 μm (H). **p = 0.0014, ****p < 0.0001 by unpaired t test.

Both proteins were present in the vascular basement membrane of wild type siblings, but at significantly diminished levels in the *spock1*[hm41/hm41] mutants (Figures 4D–4I). These data suggest that Spock1 helps induce barrier function by keeping gelatinase activity in check to allow proper deposition of necessary vascular basement membrane proteins.

Spock1 plays a conserved role in inducing barrier function in mammals

To determine whether Spock1 plays a conserved role in determining vertebrate BBB properties, we assessed BBB function in *Spock1*^{−/−} mice[46] on E15.5,[46] a stage when the cortex BBB is fully functional[4] (Figure 5A). While wild type siblings confined both 550-Da Sulfo-NHS-Biotin (Figure 5B) and 10-kDa dextran (Figure 5D) within the brain vasculature, *Spock1*^{−/−} mice leaked both tracers into the cortex parenchyma (Figures 5C–5G). This increased BBB permeability was also associated with increased expression of PLVAP (Figures 5H–5L), as seen in the zebrafish mutants (Figure 1N). These data indicate that Spock1 plays a conserved role in inducing barrier properties during embryonic development. However, when we repeated these leakage assays in adult mice, we observed full recovery in BBB function in *Spock1*^{−/−} mice (Figure S7). This contrasts with adult zebrafish *spock1*[hm41/hm41] mutants, which have a defective BBB (Figure 1G), indicating species-specific differences in the adult BBB.

Vascular cells are the only altered cell types in *spock1* mutant brains

To determine how Spock1, a neuronally produced and secreted proteoglycan, signals to and regulates brain endothelial cell BBB properties, we turned to scRNA-seq of dissected 5 dpf *spock1*[hm41/hm41] mutant and wild type brains, allowing us to globally assess cell type specific molecular changes occurring in the mutant brains. With Leiden clustering of the scRNA-seq data, we defined cell clusters

One of the proposed roles of Spock1 is to regulate matrix metalloproteinase (MMP) activation, specifically gelatinases MMP-2 and MMP-9.[35,40–43] To assess whether *spock1*[hm41/hm41] mutants had altered gelatinase activity that corresponded to observed changes in vascular cell interactions, we performed *in vivo* gelatin zymography by intracranial injections of highly quenched fluorescein isothiocyanate (FITC)-gelatin. Proteolytic cleavage of FITC-gelatin by either MMP-2 or -9 releases bright FITC peptides resulting in a non-reversible increase in fluorescence. This increase in fluorescence upon digestion is proportional to the proteolytic activity of the MMPs, allowing for the detection of gelatinase activity *in vivo*.[44,45] Using this assay, we were able to see that in wild type 5 dpf fish, the majority of the signal strongly appears in the cerebral spinal fluid (CSF) and more subtly in many pericytes (Figure 4A). While *spock1*[hm41/hm41] mutants also displayed strong gelatinase activity in the CSF, this was accompanied by a regional increase in gelatinase activity specifically in the forebrain and midbrain (Figures 4B and 4C), the same regions that were also prone to tracer accumulation (Figure 1). As MMPs are known to cleave many ECM substrates, we wondered which vascular ECM components were altered with the increased gelatinase activity in the *spock1*[hm41/hm41] mutants. To investigate this, we performed immunofluorescence staining for ECM proteins with known roles in the vascular basement membrane, fibronectin (Figures 4D–4F) and collagen IV (Figures 4G–4I).
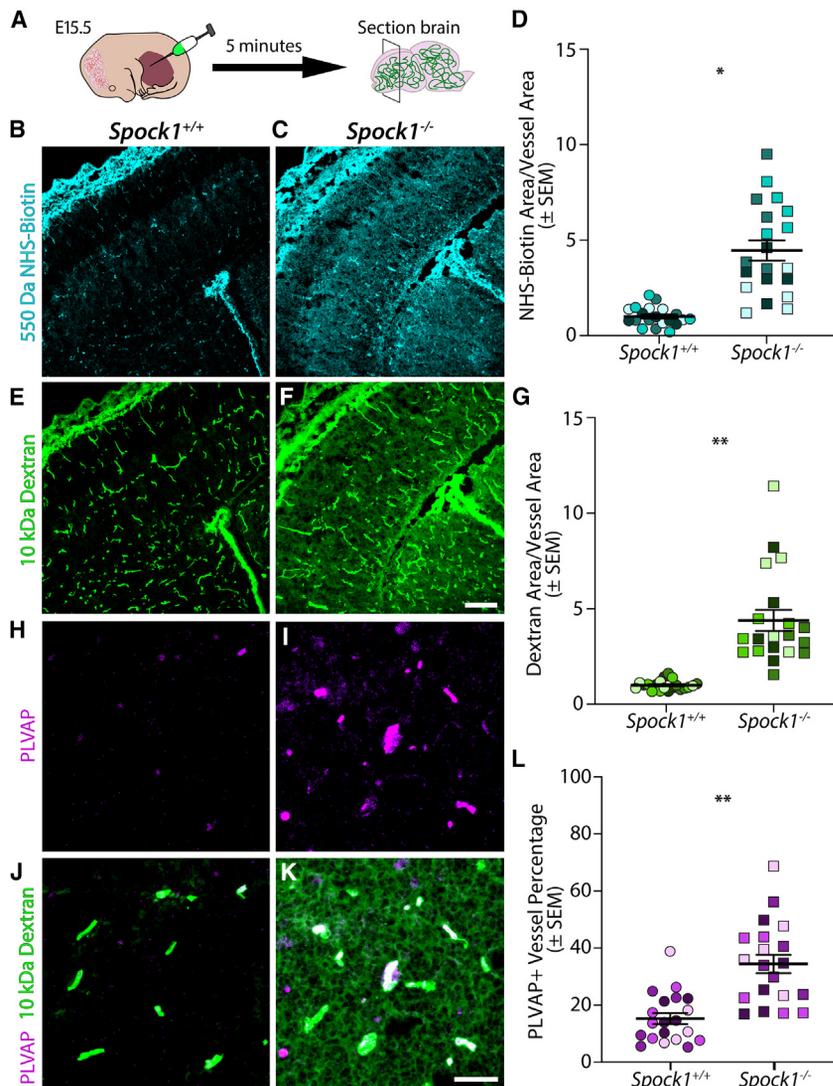
Developmental Cell
Article

Figure 5. Spock1 plays a conserved role in inducing barrier function during embryonic development in mice

(A) Schematic of functional tracer leakage assays in embryonic day 15.5 (E15.5) mice.

(B–G) Wild type mice confine both injected 550-Da NHS-Biotin (B) and 10 kDa dextran (D) within the vasculature, as previously reported. However, $Spock1^{-/-}$ mice leak both NHS-Biotin (C) and dextran (E) into the brain parenchyma. Quantification of the total area of NHS-Biotin leakage (D) and dextran leakage (G) normalized to vessel area where a ratio of 1 indicates no leakage reveals a significant increase in extravasation of both tracers in the $Spock1^{-/-}$ embryos (p = 0.0191, F and p = 0.0048, G by nested t test).

(H–L) Zoomed in view of 10-kDa dextran (green) injected embryos immunostained for the leaky vessel marker PLVAP (magenta) in wild type (H and J) reveals that the increased BBB permeability in $Spock1^{-/-}$ mice is accompanied by an increase in PLVAP expression in the vasculature (I and K). Quantification of PLVAP expression within the vasculature (L) reveals a significant increase in PLVAP expression in the $Spock1^{-/-}$ embryos (p = 0.0016 by nested t test). n = 4 embryos for each genotype, marked by unique colors, with 5 sections analyzed per embryo and shown as individual points. Scale bars represent 100 μm (F) and 50 μm (K).

containing neuronal, glial, and vascular cell types (Figure S6). We performed differential gene expression (DGE) analysis for each cluster and did not observe any changes in the neuronal or glial populations but did observe significant changes in cluster 13 (Table S2). When we subclustered cluster 13, we were able to resolve endothelial cells, pericytes and vascular smooth muscle cells (vSMCs) in addition to other cells in the brain, like the meninges, or contaminating pharyngeal arch remnants (Figure 6A). Due to the low vascular cell numbers present in the scRNA-seq data, we prioritized candidate genes that could potentially be involved in *spock1* signaling to the vasculature for subsequent validation by their fold-change in gene expression rather than statistical significance. These analyses suggested molecular changes in the mutant endothelial cells indicative of a leaky phenotype, with increased expression of *plvapb*, which we already observed in both the mutant fish (Figures 1N–1O) and embryonic knockout mice (Figures 5H–5L), and decreased expression of the tight junction protein *cldn5b* (Figure 6B; Table S3). Interestingly, *spock1* mutants had decreased

expression of the melanoma cell adhesion molecule *mcamb* (also known as CD146) in both endothelial cells and pericytes (Figures 6B and 6C), as well as a decrease in pericyte expression of the forkhead transcription factor *foxc1b* (Figure 6C). This decreased expression of *mcamb* in the vasculature was validated by HCR FISH, with significantly reduced expression in mutant midbrain endothelial cells and pericytes but normal levels in hindbrain vascular cells, which maintain BBB function in $spock1^{hm41/hm41}$ mutants (Figures 6D–6G). CD146 has previously been shown to be required for BBB integrity, as $CD146^{-/-}$ mice exhibit BBB breakdown due to decreased pericyte coverage and downstream loss of endothelial expression of Cldn5.[47] Pericyte expression of *foxc1b* was also down-regulated in the $spock1^{hm41/hm41}$ mutant midbrain (Figures 6H–6K). Pericyte-specific loss of Foxc1 in mice also results in increased BBB leakage and micro-hemorrhage.[48] Taken together, these results suggest that loss of Spock1 signaling alters pericyte identity without altering coverage.

Exogenous SPOCK1 restores barrier function

To test the ability of Spock1 to rescue the mutant leakage phenotype, we injected recombinant human SPOCK1 (rSPOCK1) protein directly into the brain of $spock1^{hm41/hm41}$ mutant larvae at 5 dpf and assessed brain permeability at 6 dpf. While control animals injected with PBS maintained high levels of brain permeability (Figure 7A), larvae that received at
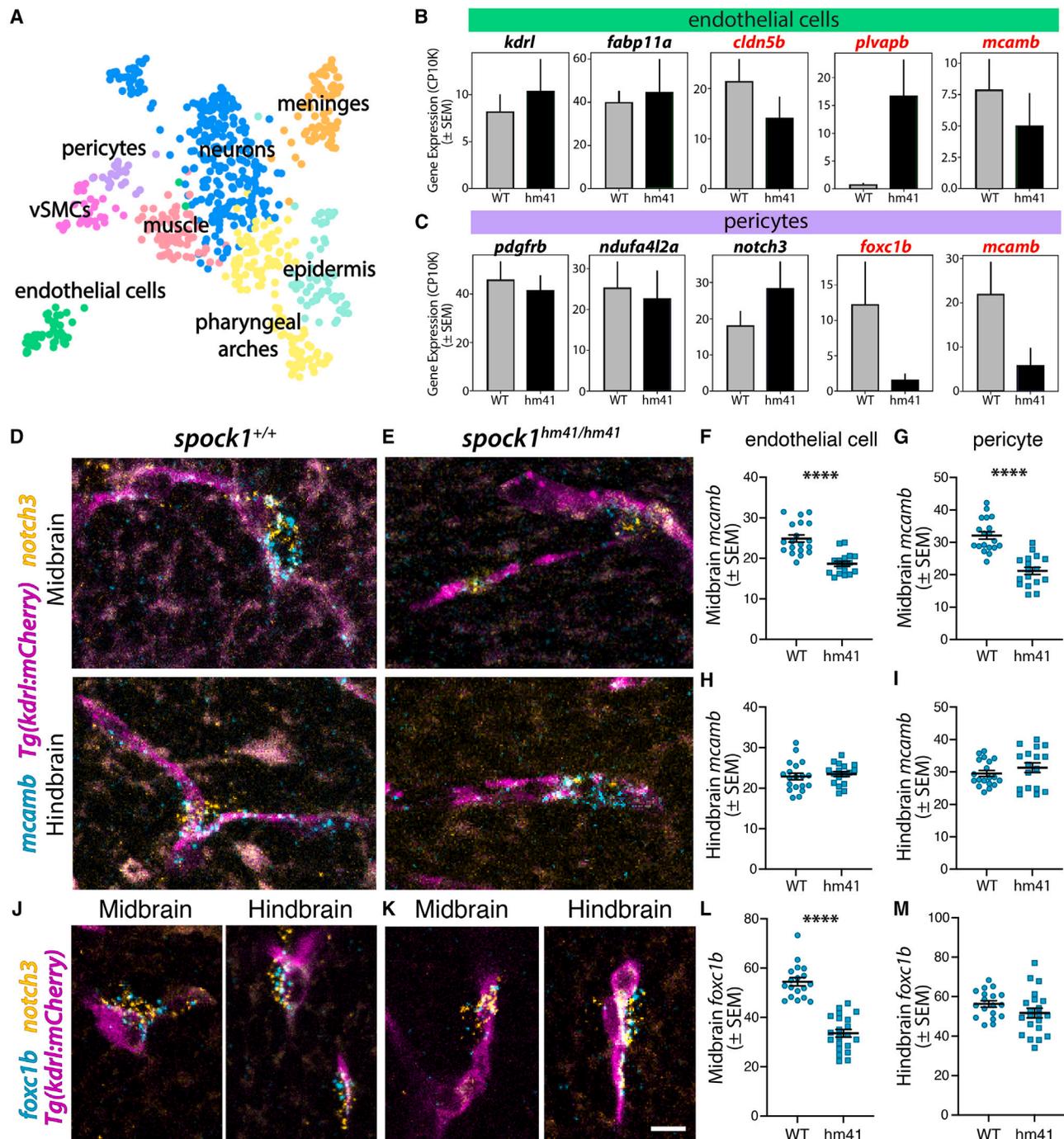
Figure 6. Spock1[hm41/hm41] mutant vascular cells have reduced expression of BBB regulators
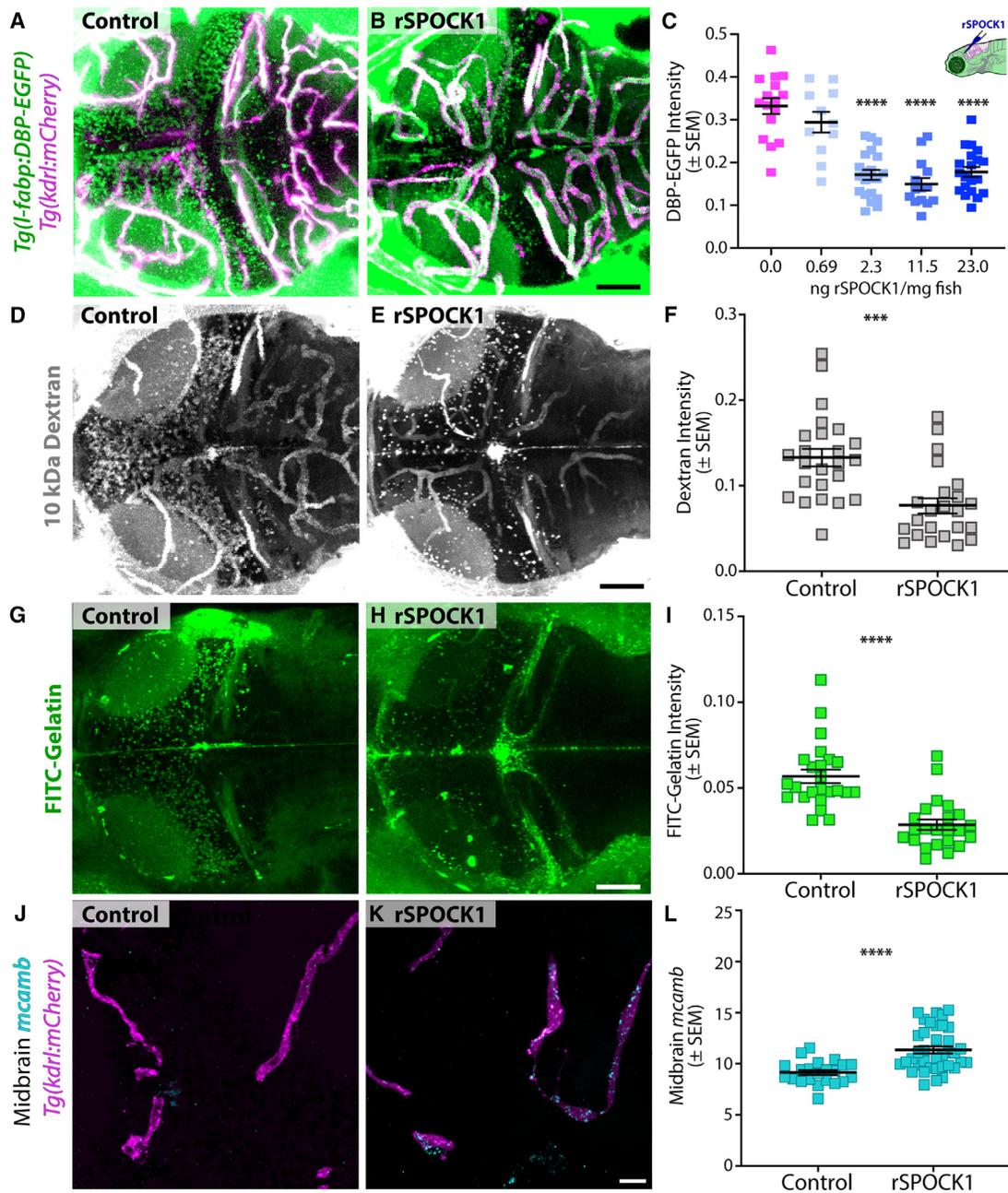
(A) UMAP of Leiden cluster 13 following subclustering and annotated by cell type, with pericytes (purple) separating from vascular smooth muscle cells (vSMCs, pink) and endothelial cells (green).

(B and C) Mean gene expression in wild type (WT, gray bars) and spock1 mutant (hm41, black bars) endothelial cells (B) and pericytes (C). Error bars represent SEM. Mutants appear to have lower levels of mcamb in both pericytes and endothelial cells and reduced foxc1b expression in pericytes.

(D–I) HCR FISH reveals strong expression of mcamb (turquoise) in wild-type vessels (magenta) and notch3+ pericytes (orange, D), both in the midbrain (F and G) and hindbrain (H and I). Spock1 mutants have significantly reduced expression of mcamb in the midbrain (E–G), but normal levels in the hindbrain (H and I), where no leakage is observed.

(J–M) HCR FISH reveals expression of foxc1b (turquoise) in wild-type notch3+ pericytes (orange, J), both in the midbrain (L) and hindbrain (M). Spock1 mutants have significantly reduced expression of foxc1b (K) in the midbrain (L) but not in the hindbrain (H).

Scale bar represents 10 μm. ****p < 0.0001 by unpaired t test.

Figure 7. Spock1 induces BBB properties by modulating the brain microenvironment, altering vascular cell biology non-autonomously

(A–C) A single intracranial injection of human rSPOCK1 into the brain at 5 dpf reduces mutant leakage of DBP-EGFP at 6 dpf about 50% (B) compared with controls injected with PBS alone (A), quantified in (C).

(D–F) Similarly, injection of rSPOCK1 at 4 dpf reduces mutant leakage of 10 kDa dextran at 5 dpf (E), quantified in (F).

(G–I) The addition of rSPOCK1 reduces gelatinase activity in the mutant brain (H) compared with control injected mutants (G), quantified in (I).

(J–L) Vascular expression of *mcamb* in the midbrain is partially restored following rSPOCK1 intracranial injections (K), quantified in (L). Scale bars represent 50 μm (C, E, and F) and 10 μm (K). ****$p < 0.0001$ by two-way ANOVA compared with PBS injected control *spock1^{hm41/hm41}* mutants in (C) and by t test in (I) and (L), ***$p < 0.001$ by t test in (F).

least 2.3 ng of rSPOCK1 per mg fish body weight showed a 50% reduction in brain permeability following a single dose (Figures 7B and 7C). These results further confirm that SPOCK1 is able to act cell non-autonomously to rescue the mutant BBB leakage, as these injections were targeted broadly to the neural tissue rather than the endothelial cells and demon-strate functional conservation of Spock1 from human to zebrafish.

To determine whether this restoration of barrier function cor-responds to Spock1's regulation of MMP activity, we repeated the intracranial injections of 11.5 ng rSPOCK1/mg of fish in *spock1^{hm41/hm41}* mutants at 4 dpf and assessed barrier function

and gelatinase activity at 5 dpf. While 5 dpf control injected *spock1*[hm41/hm41] mutants continued to display high levels of BBB permeability and gelatinase activity, rSPOCK1 reduced mutant leakage of 10 kDa dextran about 50% (Figures 7E and 7F), just as it did when we injected rSPOCK1 at 5 dpf and assessed BBB function at 6 dpf (Figure 7C). This restoration of BBB function was accompanied by a decrease in gelatinase activity (Figures 7H and 7I). Finally, to determine whether Spock1 lies upstream of vascular expression of the cell adhesion molecule *mcamb*, we assessed *mcamb* expression in the mutant midbrain vasculature at 5 dpf with or without the addition of rSPOCK1. While *spock1*[hm41/hm41] mutants injected with PBS displayed negligible levels of *mcamb* expression in the midbrain (Figure 7J), mutants injected with rSPOCK1 had a 50% increase in *mcamb* expression in the vasculature (Figures 7K and 7L), with a noticeable increase in *mcamb*+ pericytes. Interestingly this 50% increase in *mcamb* expression directly correlates with the 50% reduction in leakage and gelatinase activity following rSPOCK1 injections (Figures 7F and 7I).

DISCUSSION

Together these data show that Spock1 is a secreted, neuronally expressed extracellular signal that regulates BBB permeability in zebrafish and mouse without altering vascular patterning during development (Figures 1 and 5). Mechanistically, this work suggests a model whereby Spock1 regulates the brain extracellular environment via its inhibition of gelatinase activity, thereby providing the appropriate chemical or mechanical signals for vascular pericytes and endothelial cells to communicate properly with one another. This critical pericyte-endothelial interaction thereby prompts a BBB transcriptional program, including increased expression of tight junction (*cldn5b*) and cell adhesion (*mcamb*) molecules, decreased expression of leaky endothelial genes (*plvapb*), and reduced transcytosis. While these vascular gene expression changes are reminiscent of those observed in Wnt mutants,[20,49] we did not observe any alterations in Wnt signaling in our *spock1* mutants (Figure S1). Thus, loss of Spock1 function contributes to increased BBB permeability by disruption of the complex extracellular scaffold and cell-cell interactions required for brain vasculature during development in a Wnt-independent manner. Together this work reveals how a secreted signal from the brain microenvironment can regulate the vasculature to give rise to the special properties of the BBB and provides targets for its therapeutic modulation.

Despite the expression of *spock1* throughout the CNS, *spock1* loss-of-function zebrafish mutants display regional leakage in the forebrain and midbrain and a completely intact hindbrain barrier. Spock1 is not alone in having region-specific regulation of barrier properties despite pan-CNS expression. A recent study demonstrated that the pericyte-produced ECM molecule vitronectin is required for functional retinal and cerebellar barriers despite its expression by all CNS pericytes.[50] Even mutants in canonical Wnt signaling have varying levels or regionalized angiogenic or barrier defects despite widespread sources of Wnt signals and receptors throughout the brain.[23,25,51–55] Interestingly, the regions with the highest susceptibility to single gene mutations in canonical Wnt signaling

are the retina and the cerebellum, while the cortex can maintain a functional BBB even with mutations in several genes in the Wnt pathway.[25] These data suggest that different regions of the brain are either molecularly or cellularly (or both) distinct, perhaps in nuanced ways that are often masked by current detection methods. For example, while the NVU of endothelial cells and pericytes in close contact with astrocytic endfeet appears uniform throughout the brain by immunostaining and EM, various scRNA-seq datasets have now shown that astrocytes are highly regionally distinct at a molecular level[56–58] raising the possibility that they may respond to different signals. Pericytes in the brain, unlike in the rest of the body, arise from two discrete origins, mesodermal and neural crest.[59,60] In zebrafish, the two origins have discrete domains, with the hindbrain being exclusively derived from mesodermal origins and the midbrain and forebrain being predominantly of neural crest origin,[59] which interestingly matches the leakage boundaries in *spock1* mutants.

Here, we demonstrate that Spock1 regulates brain endothelial cell identity to initiate the barrier program during development, both at molecular and subcellular resolution. However, this does not preclude the fact that other brain barriers may be similarly affected by loss of this signal. In addition to the BBB, the neural tissue is also protected by the blood-CSF barrier, which is created by the choroid plexus epithelial cells lining the brain ventricles,[61] and the arachnoid barrier, which is created by the epithelial cells beneath the dura that completely enwrap the brain.[62] These various brain barriers mature on different developmental timelines, with the blood-CSF barrier becoming impermeable by 4 dpf,[63] then the BBB by 5 dpf,[28] and the arachnoid barrier maturing after 9 dpf[32] in zebrafish. While the focus of our study has been the BBB, it is possible that these additional brain barriers also play a role in the observed leakage of various tracers into the brain in *spock1* mutants. In fact, our scRNA-seq data suggest that the meninges of *spock1*[hm41/hm41] mutants may also be impaired with decreased expression of the tight junction *cldn11a* (Table S3), which has recently been shown to be essential for arachnoid barrier functional development.[64]

The N-terminal region of Spock1 has previously been shown to regulate MMP activity, specifically gelatinases MMP-2 and -9.[40] We show here that leaky *spock1*[hm41/hm41] mutants have increased gelatinase activity in the midbrain occurring in the same place as the observed decrease in endothelial-pericyte basement membrane (Figures 4 and S1), suggesting that this excessive MMP activity may be responsible for the breakdown of the basement membrane. Although all the cells in the NVU secrete MMP-2 and -9, pericytes have recently been shown to produce MMP-9 in response to ischemia and TGF-β1 exposure, leading to increased barrier breakdown and neuronal damage.[44,65] For this reason, many have proposed gelatinases as a therapeutic target for several neurological diseases that are accompanied with barrier breakdown including stroke, multiple sclerosis, Alzheimer's disease, and cerebral hemorrhage.[44,66–68] Given the ability of a single dose of rSPOCK1 to mitigate much of the leakage in the mutants and restore proper vascular expression of BBB genes, we propose that Spock1 may serve as a therapeutic target to reduce gelatinase activity in these neurological diseases and help restore barrier function.

Developmental Cell
Article

CellPress

Limitations of the study

While we have thoroughly characterized where *spock1* mRNA is expressed, we do not have an antibody that reliably labels Spock1 protein expression in zebrafish. This prevented us from following up further on identifying Spock1 binding partners. Furthermore, we turned to scRNA-seq to identify the mechanism of how Spock1 regulates BBB properties in an unbiased fashion, and this revealed specific changes in vascular cells and no other brain cell types. When we subclustered this cluster, we were left with only a handful of endothelial cells and pericytes and therefore focused on genes with large changes in gene expression, like *mcamb* and *foxc1b*. However, our list of differentially expressed genes in these vascular cells is not necessarily exhaustive and could be further supplemented by sorting for cell types of interest. While there are point mutations, including one missense mutation, in *hm41* mutants, it is not clear how these mutations abrogate Spock1 function.

STAR★METHODS

Detailed methods are provided in the online version of this paper and include the following:

- KEY RESOURCES TABLE
- RESOURCE AVAILABILITY
  - Lead contact
  - Materials availability
  - Data and code availability
- EXPERIMENTAL MODEL AND STUDY PARTICIPANT DETAILS
  - Zebrafish strains and maintenance
  - *Spock1*^{hm41} mutants
  - *Spock1*^{hm43} mutants
  - *TgKI(Spock1-mCherry)*^{hm44} knock-ins
  - Mouse maintenance
- METHOD DETAILS
  - Fluorescent zebrafish tracer injections and live imaging
  - Linkage mapping
  - CRISPR mutants
  - Hybridization Chain Reaction (HCR) fluorescent *in situ* hybridization (FISH)
  - Transplantation
  - Transmission electron microscopy (TEM)
  - Intracranial rSPOCK1 injections
  - In vivo gelatinase zymography
  - Zebrafish immunofluorescence staining
  - Mouse tracer injections and immunofluorescence staining
  - Single-cell RNA-sequencing
- QUANTIFICATION AND STATISTICAL ANALYSIS
  - Zebrafish permeability quantification
  - Vascular coverage
  - HCR quantification
  - Transplantation quantification
  - Gelatinase zymography
  - Zebrafish immunofluorescence
  - TEM quantification
  - Mouse permeability and PLVAP quantification

REFERENCES

1. Sweeney, M.D., Sagare, A.P., and Zlokovic, B.V. (2018). Blood–brain barrier breakdown in Alzheimer disease and other neurodegenerative disorders. Nat. Rev. Neurol. *14*, 133–150. https://doi.org/10.1038/nrneurol.2017.188.

2. Reese, T.S., and Karnovsky, M.J. (1967). Fine structural localization of a blood-brain barrier to exogenous peroxidase. J. Cell Biol. *34*, 207–217. https://doi.org/10.1083/jcb.34.1.207.

3. Campbell, M., Kiang, A.S., Kenna, P.F., Kerskens, C., Blau, C., O'Dwyer, L., Tivnan, A., Kelly, J.A., Brankin, B., Farrar, G.J., et al. (2008). RNAi-mediated reversible opening of the blood-brain barrier. J. Gene Med. *10*, 930–947. https://doi.org/10.1002/jgm.1211.

4. Ben-Zvi, A., Lacoste, B., Kur, E., Andreone, B.J., Mayshar, Y., Yan, H., and Gu, C. (2014). Mfsd2a is critical for the formation and function of the blood-brain barrier. Nature *509*, 507–511. https://doi.org/10.1038/nature13324.

5. Andreone, B.J., Chow, B.W., Tata, A., Lacoste, B., Ben-Zvi, A., Bullock, K., Deik, A.A., Ginty, D.D., Clish, C.B., and Gu, C. (2017). Blood-brain barrier permeability is regulated by lipid transport-dependent suppression of caveolae-mediated transcytosis. Neuron *94*, 581–594.e5. https://doi.org/10.1016/j.neuron.2017.03.043.

6. Hallmann, R., Mayer, D.N., Berg, E.L., Broermann, R., and Butcher, E.C. (1995). Novel mouse endothelial cell surface marker is suppressed during differentiation of the blood brain barrier. Dev. Dyn. *202*, 325–332. https://doi.org/10.1002/aja.1002020402.

7. Harik, S.I., Kalaria, R.N., Andersson, L., Lundahl, P., and Perry, G. (1990). Immunocytochemical localization of the erythroid glucose transporter: abundance in tissues with barrier functions. J. Neurosci. *10*, 3862–3872. https://doi.org/10.1523/JNEUROSCI.10-12-03862.1990.

8. Schinkel, A.H. (1999). P-glycoprotein, a gatekeeper in the blood–brain barrier. Adv. Drug Deliv. Rev. *36*, 179–194. https://doi.org/10.1016/s0169-409x(98)00085-4.

9. Sanchez-Covarrubias, L., Slosky, L.M., Thompson, B.J., Davis, T.P., and Ronaldson, P.T. (2014). Transporters at CNS barrier sites: obstacles or opportunities for drug delivery? Curr. Pharm. Des. *20*, 1422–1449.

10. Stewart, P.A., and Wiley, M.J. (1981). Developing nervous tissue induces formation of blood-brain barrier characteristics in invading endothelial cells: a study using quail-chick transplantation chimeras. Dev. Biol. *84*, 183–192. https://doi.org/10.1016/0012-1606(81)90382-1.

11. Lyck, R., Ruderisch, N., Moll, A.G., Steiner, O., Cohen, C.D., Engelhardt, B., Makrides, V., and Verrey, F. (2009). Culture-induced changes in blood-brain barrier transcriptome: implications for amino-acid transporters in vivo. J. Cereb. Blood Flow Metab. *29*, 1491–1502. https://doi.org/10.1038/jcbfm.2009.72.

12. Urich, E., Lazic, S.E., Molnos, J., Wells, I., and Freskgård, P.O. (2012). Transcriptional profiling of human brain endothelial cells reveals key properties crucial for predictive in vitro blood-brain barrier models. PLoS One *7*, e38149. https://doi.org/10.1371/journal.pone.0038149.

13. Guérit, S., Fidan, E., Macas, J., Czupalla, C.J., Figueiredo, R., Vijikumar, A., Yalcin, B.H., Thom, S., Winter, P., Gerhardt, H., et al. (2021). Astrocyte-derived Wnt growth factors are required for endothelial blood-brain barrier maintenance. Prog. Neurobiol. *199*, 101937. https://doi.org/10.1016/j.pneurobio.2020.101937.

14. Heithoff, B.P., George, K.K., Phares, A.N., Zuidhoek, I.A., Munoz-Ballester, C., and Robel, S. (2021). Astrocytes are necessary for blood–brain barrier maintenance in the adult mouse brain. Glia *69*, 436–472. https://doi.org/10.1002/glia.23908.

15. Armulik, A., Genové, G., Mäe, M., Nisancioglu, M.H., Wallgard, E., Niaudet, C., He, L., Norlin, J., Lindblom, P., Strittmatter, K., et al. (2010). Pericytes regulate the blood-brain barrier. Nature *468*, 557–561. https://doi.org/10.1038/nature09522.

16. Daneman, R., Zhou, L., Kebede, A.A., and Barres, B.A. (2010). Pericytes are required for blood-brain barrier integrity during embryogenesis. Nature *468*, 562–566. https://doi.org/10.1038/nature09513.

17. Bell, R.D., Winkler, E.A., Sagare, A.P., Singh, I., LaRue, B., Deane, R., and Zlokovic, B.V. (2010). Pericytes control key neurovascular functions and neuronal phenotype in the adult brain and during brain aging. Neuron *68*, 409–427. https://doi.org/10.1016/j.neuron.2010.09.043.

18. Abbott, N.J., Rönnbäck, L., and Hansson, E. (2006). Astrocyte–endothelial interactions at the blood–brain barrier. Nat. Rev. Neurosci. *7*, 41–53. https://doi.org/10.1038/nrn1824.

19. Janzer, R.C., and Raff, M.C. (1987). Astrocytes induce blood-brain barrier properties in endothelial cells. Nature *325*, 253–257. https://doi.org/10.1038/325253a0.

20. Benz, F., Wichitnaowarat, V., Lehmann, M., Germano, R.F., Mihova, D., Macas, J., Adams, R.H., Taketo, M.M., Plate, K.H., Guérit, S., et al. (2019). Low wnt/β-catenin signaling determines leaky vessels in the subfornical organ and affects water homeostasis in mice. eLife *8*, e43818. https://doi.org/10.7554/eLife.43818.

21. Stenman, J.M., Rajagopal, J., Carroll, T.J., Ishibashi, M., McMahon, J., and McMahon, A.P. (2008). Canonical Wnt signaling regulates organ-specific assembly and differentiation of CNS vasculature. Science *322*, 1247–1250. https://doi.org/10.1126/science.1164594.

22. Daneman, R., Agalliu, D., Zhou, L., Kuhnert, F., Kuo, C.J., and Barres, B.A. (2009). Wnt/beta-catenin signaling is required for CNS, but not non-CNS, angiogenesis. Proc. Natl. Acad. Sci. USA *106*, 641–646. https://doi.org/10.1073/pnas.0805165106.

23. Wang, Y., Rattner, A., Zhou, Y., Williams, J., Smallwood, P.M., and Nathans, J. (2012). Norrin/Frizzled4 signaling in retinal vascular development and blood brain barrier plasticity. Cell *151*, 1332–1344. https://doi.org/10.1016/j.cell.2012.10.042.

24. Vanhollebeke, B., Stone, O.A., Bostaille, N., Cho, C., Zhou, Y., Maquet, E., Gauquier, A., Cabochette, P., Fukuhara, S., Mochizuki, N., et al. (2015). Tip cell-specific requirement for an atypical Gpr124- and Reck-dependent Wnt/β-catenin pathway during brain angiogenesis. eLife *4*. https://doi.org/10.7554/eLife.06489.

25. Wang, Y., Cho, C., Williams, J., Smallwood, P.M., Zhang, C., Junge, H.J., and Nathans, J. (2018). Interplay of the Norrin and Wnt7a/Wnt7b signaling systems in blood–brain barrier and blood–retina barrier development and maintenance. Proc. Natl. Acad. Sci. USA *115*, E11827–E11836. https://doi.org/10.1073/pnas.1813217115.

26. Martin, M., Vermeiren, S., Bostaille, N., Eubelen, M., Spitzer, D., Vermeersch, M., Profaci, C.P., Pozuelo, E., Toussay, X., Raman-Nair, J., et al. (2022). Engineered Wnt ligands enable blood-brain barrier repair in neurological disorders. Science *375*, eabm4459. https://doi.org/10.1126/science.abm4459.

27. Liebner, S., Corada, M., Bangsow, T., Babbage, J., Taddei, A., Czupalla, C.J., Reis, M., Felici, A., Wolburg, H., Fruttiger, M., et al. (2008). Wnt/β-catenin signaling controls development of the blood–brain barrier. J. Cell Biol. *183*, 409–417. https://doi.org/10.1083/jcb.200806024.

28. O'Brown, N.M., Megason, S.G., and Gu, C. (2019). Suppression of transcytosis regulates zebrafish blood-brain barrier function. eLife *8*, 41. https://doi.org/10.7554/eLife.47326.

29. Xie, J., Farage, E., Sugimoto, M., and Anand-Apte, B. (2010). A novel transgenic zebrafish model for blood-brain and blood-retinal barrier development. BMC Dev. Biol. *10*, 76. https://doi.org/10.1186/1471-213X-10-76.

30. Guemez-Gamboa, A., Nguyen, L.N., Yang, H., Zaki, M.S., Kara, M., Ben-Omran, T., Akizu, N., Rosti, R.O., Rosti, B., Scott, E., et al. (2015). Inactivating mutations in MFSD2A, required for omega-3 fatty acid transport in brain, cause a lethal microcephaly syndrome. Nat. Genet. *47*, 809–813. https://doi.org/10.1038/ng.3311.

31. Umans, R.A., Henson, H.E., Mu, F., Parupalli, C., Ju, B., Peters, J.L., Lanham, K.A., Plavicki, J.S., and Taylor, M.R. (2017). CNS angiogenesis and barriergenesis occur simultaneously. Dev. Biol. *425*, 101–108. https://doi.org/10.1016/j.ydbio.2017.03.017.

32. Jeong, J.Y., Kwon, H.B., Ahn, J.C., Kang, D., Kwon, S.H., Park, J.A., and Kim, K.W. (2008). Functional and developmental analysis of the blood–brain barrier in zebrafish. Brain Res. Bull. *75*, 619–628. https://doi.org/10.1016/j.brainresbull.2007.10.043.

33. Miller, A.C., Obholzer, N.D., Shah, A.N., Megason, S.G., and Moens, C.B. (2013). RNA-seq-based mapping and candidate identification of mutations from forward genetic screens. Genome Res. *23*, 679–686. https://doi.org/10.1101/gr.147322.112.

34. Bonnet, F., Périn, J.P., Charbonnier, F., Camuzat, A., Roussel, G., Nussbaum, J.L., and Alliel, P.M. (1996). Structure and cellular distribution of mouse brain testican. Association with the postsynaptic area of hippocampus pyramidal cells. J. Biol. Chem. *271*, 4373–4380. https://doi.org/10.1074/jbc.271.8.4373.

35. Edgell, C.J., BaSalamah, M.A., and Marr, H.S. (2004). Testican-1: a differentially expressed proteoglycan with protease inhibiting activities. Int. Rev. Cytol. *236*, 101–122. https://doi.org/10.1016/S0074-7696(04)36003-1.

36. Charbonnier, F., Chanoine, C., Cifuentes-Diaz, C., Gallien, C.L., Rieger, F., Alliel, P.M., and Périn, J.P. (2000). Expression of the proteoglycan SPOCK during mouse embryo development. Mech. Dev. *90*, 317–321. https://doi.org/10.1016/s0925-4773(99)00255-5.

37. Raj, B., Farrell, J.A., Liu, J., Kholtei, J.E., Carte, A.N., Acedo, J.N., Du, L.Y., McKenna, A., Relić, Đ., Leslie, J.M., et al. (2020). Emergence of neuronal diversity during vertebrate brain development. Neuron *108*, 1058–1074.e6. https://doi.org/10.1016/j.neuron.2020.09.023.

38. Armulik, A., Genové, G., and Betsholtz, C. (2011). Pericytes: developmental, physiological, and pathological perspectives, problems, and promises. Dev. Cell *21*, 193–215. https://doi.org/10.1016/j.devcel.2011.07.001.

39. Wang, Y., Pan, L., Moens, C.B., and Appel, B. (2014). Notch3 establishes brain vascular integrity by regulating pericyte number. Development *141*, 307–317. https://doi.org/10.1242/dev.096107.

Developmental Cell
Article

CellPress

40. Du, Z., Lin, Z., Wang, Z., Liu, D., Tian, D., and Xia, L. (2020). SPOCK1 over-expression induced by platelet-derived growth factor-BB promotes hepatic stellate cell activation and liver fibrosis through the integrin α5β1/PI3K/Akt signaling pathway. Lab. Investig. *100*, 1–15. https://doi.org/10.1038/s41374-020-0425-4.

41. Ye, Z., Chen, J., Hu, X., Yang, S., Xuan, Z., Lu, X., and Zhao, Q. (2020). SPOCK1: a multi-domain proteoglycan at the crossroads of extracellular matrix remodeling and cancer development. Am. J. Cancer Res. *10*, 3127–3137.

42. Váncza, L., Tátrai, P., Reszegi, A., Baghy, K., and Kovalszky, I. (2022). SPOCK1 with unexpected function. The start of a new career. Am. J. Physiol. Cell Physiol. *322*, C688–C693. https://doi.org/10.1152/ajpcell.00033.2022.

43. Nakada, M., Yamada, A., Takino, T., Miyamori, H., Takahashi, T., Yamashita, J., and Sato, H. (2001). Suppression of membrane-type 1 matrix metalloproteinase (MMP)-mediated MMP-2 activation and tumor invasion by testican 3 and its splicing variant gene product, N-Tes. Cancer Res. *61*, 8896–8902.

44. Underly, R.G., Levy, M., Hartmann, D.A., Grant, R.I., Watson, A.N., and Shih, A.Y. (2017). Pericytes as inducers of rapid, matrix metalloproteinase-9-dependent capillary damage during ischemia. J. Neurosci. *37*, 129–140. https://doi.org/10.1523/JNEUROSCI.2891-16.2016.

45. Garcia-Alloza, M., Prada, C., Lattarulo, C., Fine, S., Borrelli, L.A., Betensky, R., Greenberg, S.M., Frosch, M.P., and Bacskai, B.J. (2009). Matrix metalloproteinase inhibition reduces oxidative stress associated with cerebral amyloid angiopathy in vivo in transgenic mice. J. Neurochem. *109*, 1636–1647. https://doi.org/10.1111/j.1471-4159.2009.06096.x.

46. Röll, S., Seul, J., Paulsson, M., and Hartmann, U. (2006). Testican-1 is dispensable for mouse development. Matrix Biol. *25*, 373–381. https://doi.org/10.1016/j.matbio.2006.05.004.

47. Chen, J., Luo, Y., Hui, H., Cai, T., Huang, H., Yang, F., Feng, J., Zhang, J., and Yan, X. (2017). CD146 coordinates brain endothelial cell–pericyte communication for blood–brain barrier development. Proc. Natl. Acad. Sci. USA *114*, E7622–E7631. https://doi.org/10.1073/pnas.1710848114.

48. Siegenthaler, J.A., Choe, Y., Patterson, K.P., Hsieh, I., Li, D., Jaminet, S.C., Daneman, R., Kume, T., Huang, E.J., and Pleasure, S.J. (2013). Foxc1 is required by pericytes during fetal brain angiogenesis. Biol. Open *2*, 647–659. https://doi.org/10.1242/bio.20135009.

49. Tam, S.J., Richmond, D.L., Kaminker, J.S., Modrusan, Z., Martin-McNulty, B., Cao, T.C., Weimer, R.M., Carano, R.A.D., Bruggen, N. van, and Watts, R.J. (2012). Death receptors DR6 and TROY regulate brain vascular development. Dev. Cell *22*, 403–417. https://doi.org/10.1016/j.devcel.2011.11.018.

50. Ayloo, S., Lazo, C.G., Sun, S., Zhang, W., Cui, B., and Gu, C. (2022). Pericyte-to-endothelial cell signaling via vitronectin-integrin regulates blood-CNS barrier. Neuron *110*, 1641–1655.e6. https://doi.org/10.1016/j.neuron.2022.02.017.

51. Zhou, Y., Wang, Y., Tischfield, M., Williams, J., Smallwood, P.M., Rattner, A., Taketo, M.M., and Nathans, J. (2014). Canonical WNT signaling components in vascular development and barrier formation. J. Clin. Invest. *124*, 3825–3846. https://doi.org/10.1172/JCI76431.

52. Xu, Q., Wang, Y., Dabdoub, A., Smallwood, P.M., Williams, J., Woods, C., Kelley, M.W., Jiang, L., Tasman, W., Zhang, K., et al. (2004). Vascular development in the retina and inner ear: control by Norrin and Frizzled-4, a high-affinity ligand-receptor pair. Cell *116*, 883–895. https://doi.org/10.1016/s0092-8674(04)00216-8.

53. Cho, C., Smallwood, P.M., and Nathans, J. (2017). Reck and Gpr124 are essential receptor cofactors for Wnt7a/Wnt7b-specific signaling in mammalian CNS angiogenesis and blood-brain barrier regulation. Neuron *95*, 1056–1073.e5. https://doi.org/10.1016/j.neuron.2017.07.031.

54. Junge, H.J., Yang, S., Burton, J.B., Paes, K., Shu, X., French, D.M., Costa, M., Rice, D.S., and Ye, W. (2009). TSPAN12 regulates retinal vascular development by promoting norrin- but not Wnt-induced FZD4/β-catenin signaling. Cell *139*, 299–311. https://doi.org/10.1016/j.cell.2009.07.048.

55. Zhou, Y., and Nathans, J. (2014). Gpr124 controls CNS angiogenesis and blood-brain barrier integrity by promoting ligand-specific canonical Wnt signaling. Dev. Cell *31*, 248–256. https://doi.org/10.1016/j.devcel.2014.08.018.

56. Zhu, Q., Shah, S., Dries, R., Cai, L., and Yuan, G.C. (2018). Identification of spatially associated subpopulations by combining scRNA-seq and sequential fluorescence in situ hybridization data. Nat. Biotechnol. https://doi.org/10.1038/nbt.4260.

57. Herrero-Navarro, Á., Puche-Aroca, L., Moreno-Juan, V., Sempere-Ferràndez, A., Espinosa, A., Susín, R., Torres-Masjoan, L., Leyva-Díaz, E., Karow, M., Figueres-Oñate, M., et al. (2021). Astrocytes and neurons share region-specific transcriptional signatures that confer regional identity to neuronal reprogramming. Sci. Adv. *7*, eabe8978. https://doi.org/10.1126/sciadv.abe8978.

58. Ohlig, S., Clavreul, S., Thorwirth, M., Simon-Ebert, T., Bocchi, R., Ulbricht, S., Kannayian, N., Rossner, M., Sirko, S., Smialowski, P., et al. (2021). Molecular diversity of diencephalic astrocytes reveals adult astrogenesis regulated by Smad4. EMBO J. *40*, e107532. https://doi.org/10.15252/embj.2020107532.

59. Ando, K., Fukuhara, S., Izumi, N., Nakajima, H., Fukui, H., Kelsh, R.N., and Mochizuki, N. (2016). Clarification of mural cell coverage of vascular endothelial cells by live imaging of zebrafish. Development *143*, 1328–1339. https://doi.org/10.1242/dev.132654.

60. Trost, A., Lange, S., Schroedl, F., Bruckner, D., Motloch, K.A., Bogner, B., Kaser-Eichberger, A., Strohmaier, C., Runge, C., Aigner, L., et al. (2016). Brain and retinal pericytes: origin, function and role. Front. Cell. Neurosci. *10*, 20. https://doi.org/10.3389/fncel.2016.00020.

61. Wolburg, H., and Paulus, W. (2010). Choroid plexus: biology and pathology. Acta Neuropathol. *119*, 75–88. https://doi.org/10.1007/s00401-009-0627-8.

62. Abbott, N.J. (2004). Evidence for bulk flow of brain interstitial fluid: significance for physiology and pathology. Neurochem. Int. *45*, 545–552. https://doi.org/10.1016/j.neuint.2003.11.006.

63. Henson, H.E., Parupalli, C., Ju, B., and Taylor, M.R. (2014). Functional and genetic analysis of choroid plexus development in zebrafish. Front. Neurosci. *8*, 364. https://doi.org/10.3389/fnins.2014.00364.

64. Derk, J., Como, C.N., Jones, H.E., Joyce, L.R., Kim, S., Spencer, B.L., Bonney, S., O'Rourke, R., Pawlikowski, B., Doran, K.S., et al. (2023). Formation and function of the meningeal arachnoid barrier around the developing mouse brain. Dev. Cell *58*, 635–644.e4. https://doi.org/10.1016/j.devcel.2023.03.005.

65. Takahashi, Y., Maki, T., Liang, A.C., Itoh, K., Lok, J., Osumi, N., and Arai, K. (2014). p38 MAP kinase mediates transforming-growth factor-β1-induced upregulation of matrix metalloproteinase-9 but not -2 in human brain pericytes. Brain Res. *1593*, 1–8. https://doi.org/10.1016/j.brainres.2014.10.029.

66. Avolio, C., Ruggieri, M., Giuliani, F., Liuzzi, G.M., Leante, R., Riccio, P., Livrea, P., and Trojano, M. (2003). Serum MMP-2 and MMP-9 are elevated in different multiple sclerosis subtypes. J. Neuroimmunol. *136*, 46–53. https://doi.org/10.1016/s0165-5728(03)00006-7.

67. Kook, S.Y., Seok Hong, H.S., Moon, M., and Mook-Jung, I. (2013). Disruption of blood-brain barrier in Alzheimer disease pathogenesis. Tissue Barriers *1*, e23993. https://doi.org/10.4161/tisb.23993.

68. Rosell, A., Cuadrado, E., Ortega-Aznar, A., Hernández-Guillamon, M., Lo, E.H., and Montaner, J. (2008). MMP-9–positive neutrophil infiltration is associated to blood–brain barrier breakdown and basal lamina type IV collagen degradation during hemorrhagic transformation after human ischemic stroke. Stroke *39*, 1121–1126. https://doi.org/10.1161/STROKEAHA.107.500868.

69. Chi, N.C., Shaw, R.M., De Val, S.D., Kang, G., Jan, L.Y., Black, B.L., and Stainier, D.Y.R. (2008). Foxn4 directly regulates tbx2b expression and atrioventricular canal formation. Genes Dev. *22*, 734–739. https://doi.org/10.1101/gad.1629408.

70. Xiong, F., Ma, W., Hiscock, T.W., Mosaliganti, K.R., Tentner, A.R., Brakke, K.A., Rannou, N., Gelas, A., Souhait, L., Swinburne, I.A., et al. (2014). Interplay of cell shape and division orientation promotes robust

morphogenesis of developing epithelia. Cell *159*, 415–427. https://doi.org/10.1016/j.cell.2014.09.007.

71. Kim, D.H., Kim, J., Marques, J.C., Grama, A., Hildebrand, D.G.C., Gu, W., Li, J.M., and Robson, D.N. (2017). Pan-neuronal calcium imaging with cellular resolution in freely swimming zebrafish. Nat. Methods *14*, 1107–1114. https://doi.org/10.1038/nmeth.4429.

72. Blader, P., Plessy, C., and Strähle, U. (2003). Multiple regulatory elements with spatially and temporally distinct activities control neurogenin1 expression in primary neurons of the zebrafish embryo. Mech. Dev. *120*, 211–218. https://doi.org/10.1016/s0925-4773(02)00413-6.

73. Wolf, F.A., Angerer, P., and Theis, F.J. (2018). SCANPY: large-scale single-cell gene expression data analysis. Genome Biol. *19*, 15. https://doi.org/10.1186/s13059-017-1382-0.

74. Schindelin, J., Arganda-Carreras, I., Frise, E., Kaynig, V., Longair, M., Pietzsch, T., Preibisch, S., Rueden, C., Saalfeld, S., Schmid, B., et al. (2012). Fiji: an open-source platform for biological-image analysis. Nat. Methods *9*, 676–682. https://doi.org/10.1038/nmeth.2019.

75. Berg, S., Kutra, D., Kroeger, T., Straehle, C.N., Kausler, B.X., Haubold, C., Schiegg, M., Ales, J., Beier, T., Rudy, M., et al. (2019). ilastik: interactive machine learning for (bio)image analysis. Nat. Methods *16*, 1226–1232. https://doi.org/10.1038/s41592-019-0582-9.

76. Weinreb, C., Wolock, S., and Klein, A.M. (2018). SPRING: a kinetic interface for visualizing high dimensional single-cell expression data. Bioinformatics *34*, 1246–1248. https://doi.org/10.1093/bioinformatics/btx792.

77. Westerfield, M. (1993). The Zebrafish Book: a Guide for the Laboratory Use of Zebrafish (Brachydanio rerio) (University of Oregon Press).

78. Li, B., and Dewey, C.N. (2011). RSEM: accurate transcript quantification from RNA-Seq data with or without a reference genome. BMC Bioinformatics *12*, 323. https://doi.org/10.1186/1471-2105-12-323.

79. Choi, H.M.T., Schwarzkopf, M., Fornace, M.E., Acharya, A., Artavanis, G., Stegmaier, J., Cunha, A., and Pierce, N.A. (2018). Third-generation in situ hybridization chain reaction: multiplexed, quantitative, sensitive, versatile, robust. Development *145*. https://doi.org/10.1242/dev.165753.

80. Pomreinke, A.P., Soh, G.H., Rogers, K.W., Bergmann, J.K., Bläßle, A.J., and Müller, P. (2017). Dynamics of BMP signaling and distribution during zebrafish dorsal-ventral patterning. eLife *6*, e25861. https://doi.org/10.7554/eLife.25861.

81. Bresciani, E., Broadbridge, E., and Liu, P.P. (2018). An efficient dissociation protocol for generation of single cell suspension from zebrafish embryos and larvae. MethodsX *5*, 1287–1290. https://doi.org/10.1016/j.mex.2018.10.009.

82. McGinnis, C.S., Patterson, D.M., Winkler, J., Conrad, D.N., Hein, M.Y., Srivastava, V., Hu, J.L., Murrow, L.M., Weissman, J.S., Werb, Z., et al. (2019). MULTI-seq: sample multiplexing for single-cell RNA sequencing using lipid-tagged indices. Nat. Methods *16*, 619–626. https://doi.org/10.1038/s41592-019-0433-8.

83. Klein, A.M., Mazutis, L., Akartuna, I., Tallapragada, N., Veres, A., Li, V., Peshkin, L., Weitz, D.A., and Kirschner, M.W. (2015). Droplet barcoding for single-cell transcriptomics applied to embryonic stem cells. Cell *161*, 1187–1201. https://doi.org/10.1016/j.cell.2015.04.044.

84. Wagner, D.E., Weinreb, C., Collins, Z.M., Briggs, J.A., Megason, S.G., and Klein, A.M. (2018). Single-cell mapping of gene expression landscapes and lineage in the zebrafish embryo. Science *108*, 981–987. https://doi.org/10.1126/science.aar4362.

85. Traag, V.A., Waltman, L., and Eck, N.J. van (2019). From Louvain to Leiden: guaranteeing well-connected communities. Sci. Rep. *9*, 5233. https://doi.org/10.1038/s41598-019-41695-z.

86. Chow, B.W., and Gu, C. (2017). Gradual suppression of transcytosis governs functional blood-retinal barrier formation. Neuron *93*, 1325–1333.e3. https://doi.org/10.1016/j.neuron.2017.02.043.

Developmental Cell
Article

CellPress

STAR★METHODS

KEY RESOURCES TABLE

REAGENT or RESOURCE	SOURCE	IDENTIFIER
Antibodies		
Mouse Anti-Fibronectin	Abcam	Cat# ab6328; RRID: AB_305428
Rabbit Anti-Collagen IV	Abcam	Cat# ab6586; RRID: AB_305584
Rat Anti-PLVAP	BD Biosciences	Cat# 553849; RRID: AB_395086
Chemicals, peptides, and recombinant proteins		
FITC-Gelatin	Biovision	Cat# M1303
recombinant human SPOCK1 protein	R&D Systems	Cat# 2327-PI-050
NHS-activated gold nanoparticles	Cytodiagnostics	Cat# CGN5K-5-1
Paraformaldehyde 20% Solution, EM Grade	VWR	Cat# 15703-S
Sodium Cacodylate Buffer, 0.2M	VWR	Cat# 11653
Aqueous Glutaraldehyde EM Grade 50%	Electron Microscopy Sciences	Cat# 16320
Dextran, Alexa Fluor 647; 10,000 MW, Anionic, Fixable	Thermo Fisher	Cat# D22914
Alexa Fluor 405 NHS Ester (Succinimidyl Ester)	Thermo Fisher	Cat# A30000
HCR v3.0 Amplifiers and Buffers	Molecular Instruments	https://www.molecularinstruments.com/hcr-rnafish-products
Agarose, low gelling temperature	Sigma	A9414
EZ-Link NHS-Biotin	Thermo Fisher	20217
Dextran, Alexa Fluor 488; 10,000 MW, Anionic, Fixable	Thermo Fisher	D22910
Streptavidin, Alexa Fluor 405 Conjugate	Thermo Fisher	S32351
N-Phenylthiourea (PTU)	Sigma	222909
Deposited data		
bulk and single cell RNA-sequencing	We collected this data	https://www.ncbi.nlm.nih.gov/geo/query/acc.cgi?acc=GSE230236
Experimental models: Organisms/strains		
Zebrafish: AB wildtype strain	Zebrafish International Resource Centre	ZDB-GENO-960809-1
Zebrafish: spock1[hm41]	This study	hm41
Zebrafish: spock1[hm43]	This study	hm43
Zebrafish: Tg(kdrl:HRAS-mCherry)[s896Tg]	Chi et al.[69]	ZDB-ALT-081212-4
Zebrafish: Tg(l-fabp:DBP-EGFP)[lri500Tg]	Xie et al.[29]	ZDB-ALT-120118-1
Zebrafish: TgBAC(pdgfrb:EGFP)[ncv22Tg]	Ando et al.[59]	ZDB-ALT-160609-1
Zebrafish:Tg(plvapb:EGFP)[sj3Tg]	Umans et al.[31]	ZDB-ALT-170816-3
Zebrafish: Tg(actb2:mem-citrine-citrine)[hm30]	Xiong et al.[70]	ZDB-TGCONSTRCT-130114-2
Zebrafish: Tg(elavl3:GCaMP6s)[a13203Tg]	Kim et al.[71]	ZDB-ALT-180502-2
Zebrafish: Tg(-3.1neurog1:GFP)[sb2Tg]	Blader et al.[72]	ZDB-ALT-030904-2
Mouse: Spock1[tm1Htmn]	Röll et al.[46]	MGI:3665280
Zebrafish: TgKI(Spock1-mCherry)[hm44]	This study	hm44
Oligonucleotides		
See Table S4		N/A
Recombinant DNA		
spock1-mCherry-KI	This study	N/A

(Continued on next page)

Continued

REAGENT or RESOURCE	SOURCE	IDENTIFIER
Software and algorithms		
SCANPY	Wolf et al.[73]	https://github.com/scverse/scanpy
Fiji	Schindelin et al.[74]	https://imagej.net/software/fiji/
Ilastik	Berg et al.[75]	https://www.ilastik.org/
SPRING	Weinreb et al.[76]	https://kleintools.hms.harvard.edu/tools/spring.html
RNAmapper	Miller et al.[33]	http://www.rnamapper.org/

RESOURCE AVAILABILITY

Lead contact
Further information and requests for resources and reagents should be directed to and will be fulfilled by the lead contact, Natasha O'Brown (natasha.obrown@rutgers.edu)

Materials availability
Zebrafish lines and plasmids generated in this study will be shared by the lead contact upon request.

Data and code availability
Single-cell and bulk RNA-seq data have been deposited at GEO and are publicly available (GEO: GSE230236). All original code for the single-cell analysis is available as interactive Jupyter notebooks here: https://doi.org/10.5281/zenodo.7955159. Interactive exploration of the full single-cell data can be found here: https://kleintools.hms.harvard.edu/tools/springViewer_1_6_dev.html?client_datasets/2021_OBrown/2021_OBrown. Exploration of the cluster 13 subcluster cells can be found here: https://kleintools.hms.harvard.edu/tools/springViewer_1_6_dev.html?client_datasets/2021_OBrown_Vasculature/2021_OBrown_Vasculature. Microscopy data reported in this paper will be shared by the lead contact upon request. Any additional information required to reanalyze the data reported in this work paper is available from the lead contact upon request.

EXPERIMENTAL MODEL AND STUDY PARTICIPANT DETAILS

Zebrafish strains and maintenance
Zebrafish were maintained at 28.5°C following standard protocols.[77] All zebrafish work was approved by the Harvard Medical Area Standing Committee on Animals under protocol number IS00001263-3. Adult fish were maintained on a standard light-dark cycle from 8 am to 11 pm and fed a mix of live artemia and tropical fish granules. Adult fish, age 3 months to 2 years, were crossed to produce embryos and larvae. For imaging live larvae, 0.003% phenylthiourea (PTU) was used beginning at 1 dpf to inhibit melanin production. These studies used the AB wild-type strains and the transgenic reporter strains *Tg(l-fabp:DBP-EGFP)*[lri500Tg] abbreviated as *Tg(l-fabp:DBP-EGFP)*,[29] (*Tg(kdrl:HRAS-mCherry)*[s896Tg] abbreviated as *Tg(kdrl:mCherry)*,[69] *TgBAC(pdgfrb:EGFP)*[ncv22Tg] abbreviated as *TgBAC(pdgfrb:EGFP)*,[59] *Tg(plvapb:EGFP)*[sj3Tg] abbreviated as *Tg(plvapb:EGFP)*,[31] *Tg(actb2:mem-citrine-citrine)*[hm30] abbreviated as *Tg(actb2:mem-Citrine)*,[70] *Tg2(elavl3:GCaMP6s)*[a13203Tg] abbreviated as *Tg(elavl3:GCaMP6s)*,[71] and *Tg(-3.1neurog1:GFP)*[sb2Tg] abbreviated as *Tg(-3.1neurog1:GFP)*[72] in the text.

Spock1[hm41] mutants
Spock1[hm41] mutants were maintained in the double transgenic Tg(*l-fabp:DBP-EGFP; kdrl:mCherry*) background. Heterozygous fish were intercrossed for all leakage assays, with the exception of the time lapse microscopy experiments, where a heterozygous fish was crossed to a homozygous mutant, and the cell transplantation experiments, where homozygous mutants were in-crossed. All larvae were imaged prior to genotyping to identify wild type and mutant fish. The *spock1*[hm41] mutant line was genotyped using primers 1 and 2 (See Table S4) followed by a HaeIII restriction digest, which does not digest the wild-type product (327 bp).

Spock1[hm43] mutants
Spock1[hm43] mutants were generated and maintained in the double transgenic Tg(*plvapb:EGFP; kdrl:mCherry*) background using CRISPR mutagenesis with two sgRNAs (spock1_1 and spock1_2, Table S4) to target the *spock1* 5' UTR and start codon. Heterozygous fish were intercrossed for all leakage assays. All larvae were imaged prior to genotyping to identify wild type and mutant fish. The *spock1*[hm43] mutant line was genotyped using primers 3 and 4 (Table S4) and KAPA HiFi Hotstart polymerase (Roche:KK2602) using a 58°C annealing temperature. The mutant PCR product of 364 bp was easily distinguishable by gel electrophoresis from the wild type product at 935 bp.

Developmental Cell
Article

🔗 CellPress

TgKI(Spock1-mCherry)^{hm44} knock-ins

TgKI(Spock1-mCherry)^{hm44} knock-ins were generated and maintained in the AB background by injecting Cas9 mRNA (TriLink Bio-technologies; 100 ng/μl), crRNA:tracrRNA duplexes to target the first exon of *spock1* (spock1_KI, Table S4) and the universal gRNA site in the donor plasmid (ugRNA, Table S4) (IDT DNA Technologies; 25 μM), and a donor plasmid with 30 bp homology arms to *spock1* exon 1 (spock1-mCherry-KI; 25 ng/μl). F0 injected larvae with mCherry expression were raised to adulthood and out-crossed to find a founder with germ-line transmission as assessed by mCherry fluorescence. These F1 fish were then raised and out-crossed to other transgenic cell-type reporter lines as heterozygotes for the assessment of *spock1* expression *in vivo*. Genomic inte-gration in the correct locus was validated with PCR on genomic DNA using primers 5 and 6 (Table S4) followed by sequencing with primer 5.

Mouse maintenance

Spock1$^{-/-}$ knockout mice[46] were obtained from Ursula Hartmann's lab and were backcrossed to and maintained on a C57Bl/6 back-ground. Mice were maintained on 12 light/12 dark cycle and given LabDiet 5053 and water ad libitum. Adult mice were housed with a maximum of 5 mice per cage. Mice were genotyped with primers 7-9 (Table S4) using KAPA HiFi Hotstart polymerase (Roche:KK2602). This PCR reaction produced a 185 bp wild type band and a 750 bp knockout band in heterozygous animals. All animals were treated according to institutional and US National Institutes of Health (NIH) guidelines approved by the Institutional An-imal Care and Use Committee (IACUC) at Harvard Medical School under protocol IS00000045-6.

METHOD DETAILS

Fluorescent zebrafish tracer injections and live imaging

Larvae were immobilized with tricaine and placed in an agarose injection mold with their hearts facing upwards. 2.3 nl of Alexa Fluor 405 NHS Ester (Thermo Fisher: A30000) or Alexa Fluor 647 10 kDa Dextran (Thermo Fisher: D22914) fluorescently conjugated tracers (10 mg/ml) were injected into the cardiac sac using Nanoject II (Drummond Scientific, Broomall, PA). Larvae were then mounted with 1.5% low gelling agarose (Sigma: A9414) in embryo water on 0.17 mm coverslips and imaged live within 2 h post injection on a Leica SP8 laser scanning confocal microscope using the same acquisition settings with 1 μm z-steps using a 25x water immersion objec-tive with 0.75x magnification. Using these settings, we were able to image the entire brain of each fish. Pericyte and vascular double transgenics were similarly imaged on the Leica SP8 for quantification of vascular defects. Additional images were taken on a Zeiss LSM 980 with Airyscan 2 with 0.21 μm z-steps using a 20x water immersion objective for increased cellular resolution, allowing us to detect gaps between the two cell types in vivo.

Linkage mapping

Larvae from 2 separate crosses were screened for leakage of DBP-EGFP at 5 dpf and pooled into 3 groups of 5 to 6 leaky or wild type heads. RNA was extracted from the pools using the RNeasy mini kit and ribo-depleted. RNA sequencing libraries were prepared us-ing Wafergen Directional RNA-Seq kits and sequenced on NextSeq High-Output sequencers producing 75 bp paired end reads. Reads were mapped to the GRCz11 genome using tophat and bowtie2. Linkage mapping was performed on the mapped reads using RNAmapper[33] with the following specifications: zygosity=25, coverage=1, linkedRatio=0.96, neighbors=10. Differential gene expres-sion analysis was performed on these libraries using rsem.[78]

CRISPR mutants

Gstp2 crispant fish were generated by injection of Cas9 protein and 3 guide RNAs (gstp2_1-3; Table S4) into 1-cell fertilized double transgenic Tg(l-fabp:DBP-EGFP; kdrl:mCherry) embryos. *Csf1ra* crispant fish were generated similarly with 4 guide RNAs (csf1ra_1-4; Table S4), as were *spock1* crispants (spock1_3-6; Table S4). F0 crispants were analyzed for leakage of the DBP-EGFP tracer outside of the kdrl:mCherry labeled vasculature at 5 dpf.

Hybridization Chain Reaction (HCR) fluorescent *in situ* hybridization (FISH)
Slide

HCR RNA *in situ* hybridization (Molecular Instruments) experiments on 14 μm cryosections of fixed 5 dpf larvae were performed as previously described.[28,79] Briefly, sections were air dried and re-fixed in 4% paraformaldehyde (PFA) in PBS for 10 min at room tem-perature. Following fixation, slides were washed in PBS and then permeabilized using 1 μg/ml Proteinase K (ThermoFisher) for 5 min, followed by PBS washes and refixation. Tissues were further permeabilized by an ethanol dehydration series of 50%, 70% and two rounds of 100% ethanol and air dried for 5 min. Dried slides were put into probe hybridization solution for at least 10 min at 37°C. Subsequently, the probes for *spock1* and *mcamb* (Table S4, IDT DNA oPools) were added to the slides at a final concentration of 4 nM to hybridize overnight at 37°C. The next day, slides were washed with a series of wash buffer to 5x SSCT (5x SSC with 0.1% Tween 20). Excess liquid was then removed and samples were immersed in amplification buffer at room temperature for 30 min prior to hairpin amplification, which occurred overnight at room temperature. Slides were then washed in 5x SSCT, washed in 5x SSC and mounted with Fluoromount-G (Electron Microscopy Sciences).

Whole mount

Larvae were fixed in 4% PFA overnight and then stored in methanol at -20°C until staining was performed and within 6 months post fixation. All staining was performed in PCR strip tubes. Larvae were rehydrated in a series of methanol/PBST (0.1% Tween) washes and then permeabilized with 30 μg/ml Proteinase K for 45 min at room temperature. Larvae were then refixed in freshly made 4% PFA for 20 min and treated with probe hybridization buffer at 37°C. Subsequently, the *spock1, elavl3, mcamb, notch3, foxc1b, slc17a6b*, or *gad1b* probes (Table S4, IDT DNA oPools and Molecular Instruments) were added at a final concentration of 4 nM to hybridize 24–72 h rocking at 37°C. The next day, larvae were washed with a series of wash buffer to 5x SSCT (5x SSC with 0.1% Tween 20). Excess liquid was then removed and samples were immersed in amplification buffer at room temperature for 30 min prior to hairpin amplification, which occurred overnight rocking at room temperature at concentration of 15 pmol. Larvae were then washed and imaged in 5x SSCT.

Transplantation

Donor embryos were injected with 2.3 nl of 10 mg/ml Alexa Fluor 647 10 kDa Dextran (Thermo Fisher: D22914) at the 1-cell stage to distinguish them from host cells. Following injection, embryos were incubated at 28.5°C until transplantation. Host and donor embryos were dechorionated with 1 mg/ml Pronase (Roche:11459643001) at oblong stage and transferred to transplantation agarose dishes in 1/3 Ringer's buffer. Unfertilized or injured embryos were discarded. To generate clonal sources secreting wild type or mutant Spock1, approximately 40–80 cells were transplanted from sphere stage dextran labeled donor embryos into sphere stage wild type and mutant hosts (similar to previous studies).[80] Embryos recovered overnight in 1/3 Ringer's buffer and were subsequently transferred to Danieau Buffer with PTU. Tracer injections were performed at 5 dpf, as described above, with 1 kDa Alexa Flour 405 NHS Ester.

Transmission electron microscopy (TEM)

Larvae (7 dpf) were anesthetized with tricaine and injected with 2.3 nl of 5 nm NHS-activated gold nanoparticles (Cytodiagnostics: CGN5K-5-1, ~1.1[14] particles/ml in PBS) just as for the fluorescent tracer injections. After 5 min of circulation, the larvae were initially fixed by immersion in 4% paraformaldehyde (VWR:15713-S) /0.1M sodium cacodylate (VWR:11653). Following this initial fixation, larvae were further fixed for 7 days in 2% glutaraldehyde (Electron Microscopy Sciences: 16320)/ 4% paraformaldehyde/ 0.1M sodium cacodylate at room temperature. Following fixation, larvae were washed overnight in 0.1M sodium cacodylate. Entire larval heads were post-fixed in 1% osmium tetroxide and 1.5% potassium ferrocyanide, dehydrated, and embedded in epoxy resin. Ultrathin sections of 80 nm were then cut from the block surface and collected on copper grids.

Intracranial rSPOCK1 injections

Larvae were anesthetized with tricaine and placed in an agarose injection mold with their heads facing upwards. 2.3 nl of recombinant human SPOCK1 (rSPOCK1; R&D Systems: 2327-PI-050) at a range of 0.001-10 mg/ml was injected directly into the midbrain using Nanoject II (Drummond Scientific, Broomall, PA). Following injections, larvae recovered in normal embryo water for 1 day. The effects of rSPOCK1 were either assessed in live fish using functional tracer leakage assays and in vivo gelatin zymography or in fixed samples followed by slide HCR *in situ* hybridization, as described above.

In vivo gelatinase zymography

Larvae were anesthetized and intracranially injected as for rSPOCK1 with 2.3 nl of FITC-Gelatin (Biovision: M1303) at 5 mg/ml. After 1 h, larvae were also injected with 10 kDa Dextran in the cardiac sac to assess BBB function and then mounted with 1.5% low gelling agarose (Sigma: A9414) in embryo water on 0.17 mm coverslips and imaged live within 2 h post injection on a Leica SP8 laser scanning confocal microscope using the same acquisition settings with 1 μm z-steps and a 25x water immersion objective.

Zebrafish immunofluorescence staining

Immunofluorescence staining was performed on 14 μm thick cryosections of paraformaldehyde (4% in PBS) fixed 5 dpf wild type and mutant larvae. Slides were air dried for at least 20 min at room temperature and then washed twice with PBS. Sections were then blocked in 10% normal goat serum (NGS) in PBST (0.1% Tween) for 2 h at room temperature. Antibodies against Fibronectin (Abcam: ab6328) and Collagen IV (Abcam: ab6586) were used at 1:200 in the same blocking solution and applied overnight at 4°C. Sections were then washed in PBST several times followed by treatment with fluorescently-conjugated secondary antibodies (Jackson Immunoresearch) at 1:500 in the same blocking buffer at room temperature.

Mouse tracer injections and immunofluorescence staining

Heterozygous Spock1^{+/-} mice were intercrossed and used for tracer leakage assays performed at embryonic day 15.5 (E15.5) as previously described.[4] In brief, 5 μl of tracer cocktail (10 mg/ml EZ-Link NHS-Biotin (Thermo Fisher: 20217) and 5 mg/ml 10 kDa Dextran Alexa Fluor 488 (Thermo Fisher: D22910)) was injected into the liver of each embryo and allowed to circulate for 5 min. Embryonic heads were fixed by immersion in 4% paraformaldehyde overnight at 4°C and then frozen in TissueTek OCT (Sakura). 20 μm thick sections were then collected and immunostained with Streptavidin Alexa Fluor 405 (1:200; Thermo Fisher: S32351) and rat anti-PLVAP (1:200; BD Biosciences:553849). All embryos were injected and fixed for processing blind before genotyping. Adult mice were retroorbitally injected with 0.5 mg of EZ-Link NHS-Biotin per g of mouse body weight. The NHS-Biotin circulated for 30 min prior to

Developmental Cell
Article

CellPress

brain dissections and fixation with 4% PFA. 30 μm thick cryosections were then collected and immunostained with Streptavidin Alexa Fluor 568 (1:200; Thermo Fisher: S32351) and goat anti-CD31 (1:100; R&D Systems: AF3628).

Single-cell RNA-sequencing

Larval zebrafish brains were dissected and split along the midbrain-hindbrain boundary in DMEM. Brains were dissociated using a modified protocol.[81] Briefly, chemical dissociations were performed at 30.5°C using a mixture of 0.25% Trypsin-EDTA, Collagenase/Dispase (8 mg/mL) and DNaseI (20 μg/mL) for 15–20 min with gentle pipetting every few minutes and quenched with 10% fetal bovine serum in DMEM. Samples were hashed using Multi-seq as previously described with slight modifications.[82] For each sample, 80 pmoles of lipid modified oligos (LMOs) were used to hash every 500k cells. The hashing reaction was quenched using 1% BSA in PBS and barcoded samples were subsequently pooled and washed with 1% BSA. The pooled cell mixture was resuspended in PBS + 0.1%BSA + 18% Optiprep at a final concentration of ~300k cells/mL prior to single-cell capture with inDrops. The Single-cell Core (SCC) at Harvard Medical School captured single-cell transcriptomes and prepared NGS libraries as previously described[83] with a target capture of 45k cells per experiment.

Gene expression and hashtag libraries were mixed (9:1 ratio) and sequenced on an Illumina Nova-seq 6000 with the NovaSeq S2 kit. Reads were mapped onto the Zebrafish GRCz11 Release 101 genome assembly using previously described methods.[84] Hashtags were identified using custom code relying largely on SCANPY,[73] and available on: https://doi.org/10.5281/zenodo.7955159.

Transcriptomes with greater than 350 UMIs were further filtered for viability by removing cells with >20% mitochondrial reads. Cell demultiplexing was performed manually by applying thresholds to delineate single cells from background and multiple populations. The resulting counts matrix was normalized to the mean UMIs per cell in the dataset.

To visualize the data, we first mean-normalized the data and identified highly variable genes from the wild type AB and RNF datasets (minimum of 3 transcripts per cell, minimum of 3 cells expressing gene, minimum V-score percentile of 85%). We then Z-scored counts for each gene and performed principal component analysis (PCA) with 50 components. Cells from the spock1 mutant libraries were projected into the same principal component subspace. A k-nearest neighbor graph (k=10) was generated based on the Euclidean distance in gene expression between cells within this subspace. The Leiden algorithm was used to cluster cells into subgroups.[85] The neighborhood graph was embedded and visualized using UMAP and the data was explored interactively with SPRING[76] to aid in cell cluster annotation.

Cells belonging to the liver, pharyngeal arches, skin, and muscle were removed prior to differential gene expression (DGE) analysis. The filtered dataset was reanalyzed using the methods described above. The Wilcoxon rank-sum test was used to generate a list of potential genes that are differentially regulated (fold change > 2) between genotypes across each Leiden cluster (Table S2). Genes were only considered for DGE analysis if they were expressed in at least 5% of cells in a given cluster and had a minimum mean of 10 transcripts per cell. Cells belonging to the AB and RNF background were treated as a single wild type genotype for the analysis. The vascular cluster (Leiden 13) was subclustered and similarly analyzed for DGE (Table S3).

QUANTIFICATION AND STATISTICAL ANALYSIS

Zebrafish permeability quantification

All quantification was performed on blinded image sets. For static images, parenchymal fluorescent tracer intensity was measured using Fiji[74] in the entire regional parenchyma outside of the vasculature in 60 μm thick maximum intensity projections (MIPs) of the larval brains. These projections began on average 15 μm below the mesencephalic vein to reduce the effects of potential leakage diffusion from the surface vessels and had the vasculature masked and removed for average intensity quantification. These parenchymal tracer intensity values of the entire larval brains were then background subtracted and normalized to the tracer intensity within the vasculature to account for differential amounts of circulating tracer between fish. The average midbrain parenchymal tracer intensity for each individual fish was plotted as a single point for all tracer leakage assays. For time lapse imaging, Dextran intensity was measured in six parenchymal regions of average intensity projections of the time lapse videos and averaged as a single value per fish and similarly normalized to the average blood vessel luminal fluorescence intensity at each time point.

Vascular coverage

80 μm thick MIPs of the entire larval brain were measured for vascular and pericyte coverage using Fiji[74] as total masked vascular or pericyte area divided by total brain area.

HCR quantification

To measure levels of mcamb expression in endothelial cells and pericytes, we made 20 μm thick MIPs from the whole mount larvae and manually traced kdrl+ endothelial cells and notch3+ pericytes and measured average intensity within each cell type using Fiji on blinded image sets. On average, 4 vessels and pericytes were measured for each region (midbrain and hindbrain) and averaged into a single value for each individual fish. Similar measurements were performed for foxc1b expression in notch3+ pericytes. Quantification of spock1 co-localization with neuronal markers (elavl3, slc17a6b, and gad1b) was performed on 2.5 μm thick MIPs of the dorsal midbrain. We first used Ilastik[75] to segment individual cells in the brain based on the transgenic mem-Citrine signal. Taking this cell mask, we then measured average spock1 and other neuronal gene levels per segmented cell using the Fiji BioImaging and Optics

Platform (BIOP) plugin. Additional images were taken on a Zeiss LSM 980 with Airyscan 2 with 0.21 μm z-steps using either a 20x or a 40x water immersion objective to further enhance the resolution of the *mcamb* signal.

Transplantation quantification

Blinded image sets were analyzed using Fiji. We took each z-stack of an individual larval brain and generated 10 μm thick MIPs to span the entire brain, with an average of 10 MIPs analyzed per individual fish. Using these MIPs, we then measured average NHS tracer intensity in an 8 μm wide rectangle between donor cells and the nearest blood vessel and normalized to average blood vessel tracer intensity. We then binned tracer measurements by distance (D) to the nearest donor cell (0, 2, 4, 6, 8, 10, 12, 15, 20, and 30+ μm) and took the median tracer intensity value for each bin per individual fish. All analyzed fish had at least 1 donor cell per each distance bin.

Statistics were calculated using 2way ANOVA comparing to WT→WT at every distance bin. Mean values per each bin were plotted per genotype with standard error bars.

Gelatinase zymography

All quantification was performed on blinded 80 μm thick MIPs of the entire larval brain. Average parenchymal FITC-Gelatin probe intensity was measured using Fiji in the entire midbrain tectum and normalized to the average intensity in the ventricles, which have high gelatinase activity, to account for fish to fish injection variation. Regions of obvious damage at the injection site were excluded for quantification.

Zebrafish immunofluorescence

Images were collected with a Leica SP8 and the same settings were used across samples. Vessels were masked with the transgenic *kdrl:mCherry* signal in MIPs of the entire 14 μm thick z-stacks and used to quantify average fluorescence intensity of each ECM component within the vasculature in Fiji. Background levels of fluorescence in the surrounding brain tissue were subtracted from the average vessel intensity for each fish.

TEM quantification

Grids were imaged using a 1200EX electron microscope (JEOL) equipped with a 2k CCD digital camera (AMT) and quantified using Fiji.[74] Vesicular density values were calculated from the number of non-clathrin coated small vesicles less than 100 nm in diameter or large vesicles greater than 200 nm in diameter per μm^2 of endothelial area for each image collected. Average pericyte basement membrane (BM) thickness was quantified by measuring the total BM area divided by the length of the pericyte-endothelial contact. All images for analysis were collected at 12000x magnification. 10-15 vessels were quantified for each fish, with each color representing a different fish.

Mouse permeability and PLVAP quantification

Using a Leica SP8 with a 25x water immersion objective, we collected z-stacks spanning 20-30 μm thick sections using the same settings across samples. We collected 5 separate images for each sample. Quantification of tracer permeability into the brain parenchyma was performed on blinded MIPs using a previously reported Fiji permeability macro[86] that measures the total area of thresholded tracer signal and divides that by vascular area for each image. The same macro was used to quantify area of PLVAP+ vessels and divided by total vessel area

Supplemental information

The secreted neuronal signal Spock1

promotes blood-brain barrier development

Natasha M. O'Brown, Nikit B. Patel, Ursula Hartmann, Allon M. Klein, Chenghua Gu, and Sean G. Megason
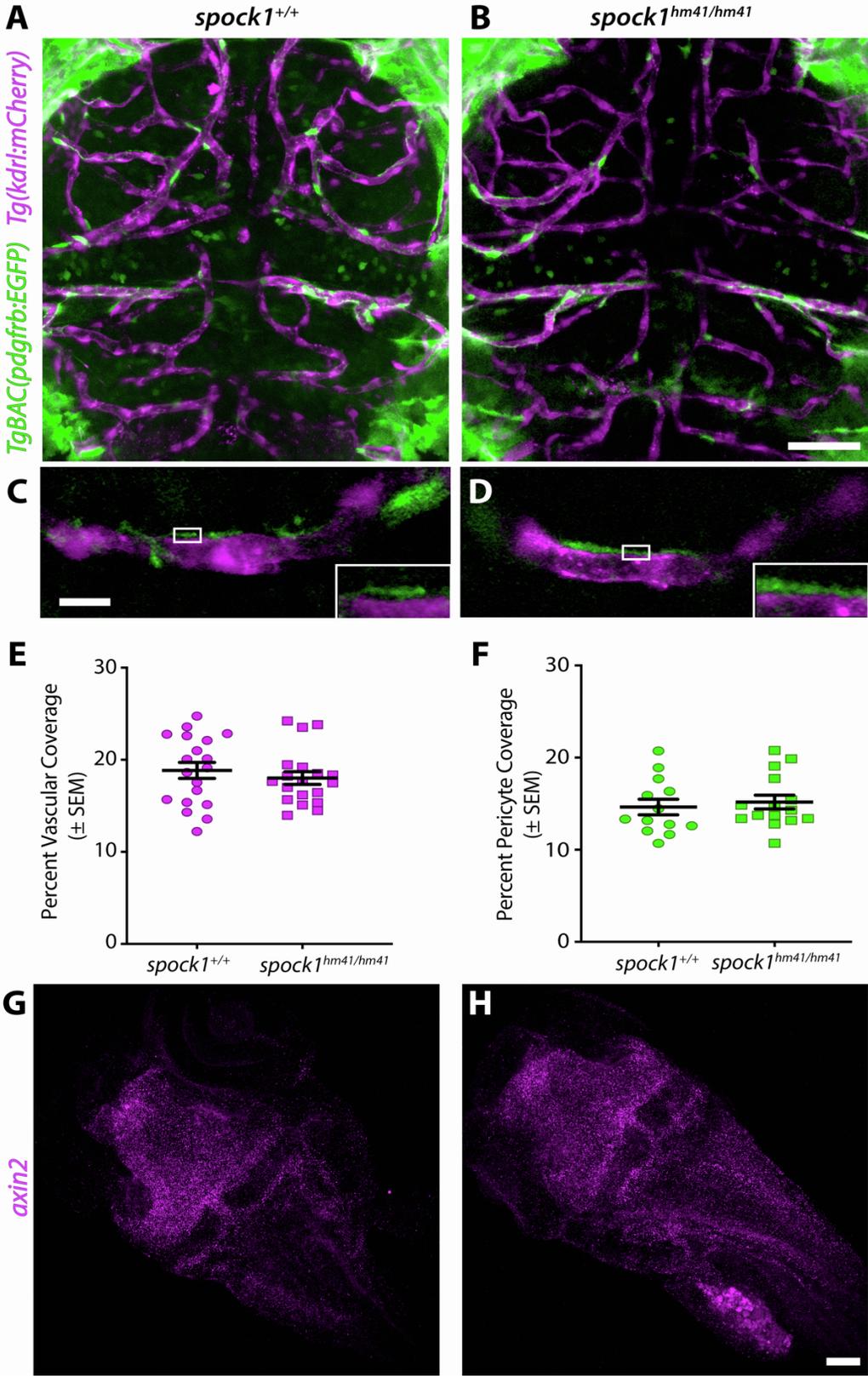
Figure S1. *Spock1^{hm41/hm41}* **mutants have normal vascular patterning and Wnt signaling, related to Figure 1.** (**A-B**) Dorsal maximum intensity projection of 5 dpf wild type (A) and mutant

(B) brains with endothelial cells marked by the kdrl:mCherry transgene (magenta) and pericytes marked by the pdgfrb:EGFP transgene (green). (**C-D**) Zoomed in view of vessels reveals diminished basement membrane between pericytes (green) and vessels (magenta) in mutants (D) compared to wild type siblings (C). This is further highlighted in the higher magnification insets, with a visible gap present in the wild type vessel (C) but not in the mutants (D). (**E-F**) Quantification of total vascular coverage of the brain (kdrl:mCherry+ area/total brain area, E) and total pericyte coverage of the vasculature (pdgfrb:EGFP+ area/kdrl:mCherry+ area, F), with each individual fish marked by a single point. (**G-H**) HCR in situ hybridization reveals similar *axin2* expression in wild type (G) and mutant brains (H), suggesting that mutant brains have normal Wnt signaling. Scale bars represent 50 µm (B, H) and 10 µm (C). T-test comparison reveals no significant difference between wild type and mutant fish for either vascular or pericyte coverage.
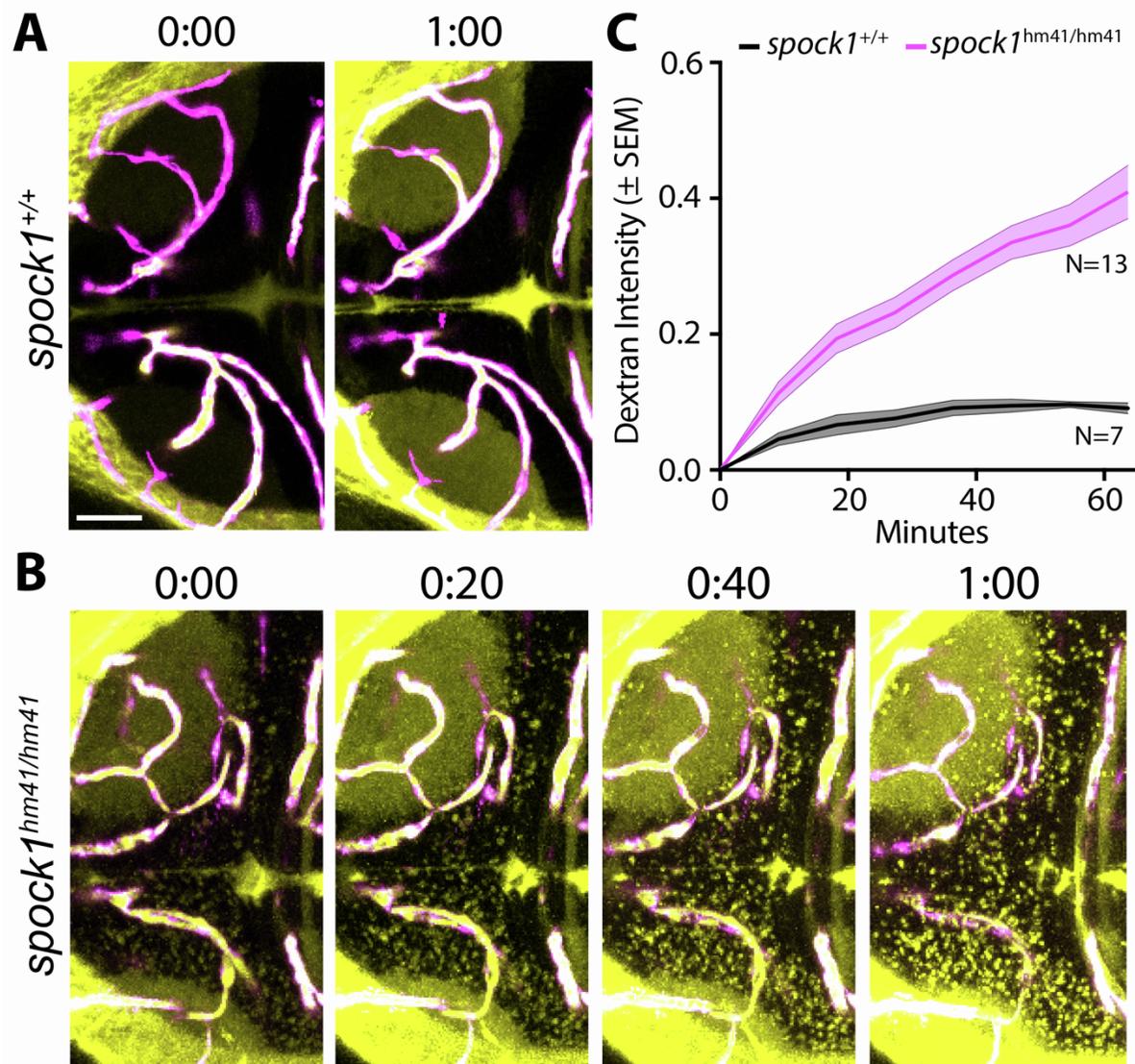
Figure S2. Time lapse imaging reveals leakage dynamics in *spock1^hm41/hm41^* mutants, related to Figure 1. (**A-B**) Dorsal maximum intensity projection of a wild type (A) and *spock1^hm41/hm41^* mutant (B) midbrain reveals steady accumulation of 10 kDa Dextran (yellow) outside of the vasculature (magenta) over the course of one hour in *spock1* mutants. (**C**) Quantification of Dextran accumulation in the midbrain parenchyma outside of the vasculature over time in wild type fish (black line) and *spock1^hm41/hm41^* mutants (magenta line). Scale bar represents 50 µm.
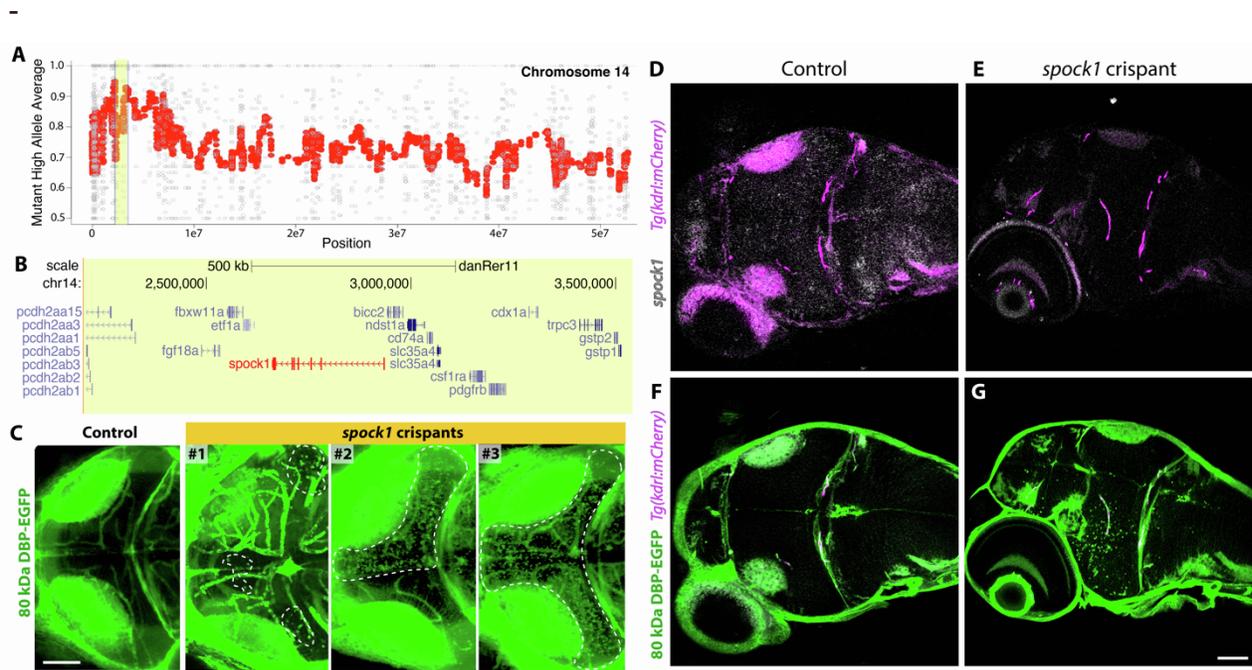
Figure S3. Leaky phenotype maps to *spock1* gene on chr14:2205271-3513919, related to Figure 1. (**A**) Manhattan plot of linkage on chromosome 14 with the average mutant alleles per 20 neighbors plotted in red. The region of highest linkage is highlighted in yellow. (**B**) Genome browser view of the highest linked region to the leaky phenotype. Eight of the genes within this region were expressed in the 5 dpf bulk RNAseq data: *fgf18a, spock1, bicc2, csf1ra, ndst1a, slc35a4, gstp1* and *gstp2*. Two of these genes were differentially expressed in leaky mutants compared to wild type (*csf1ra* and *gstp2*) and *spock1* (marked in red) had several SNPs that completely segregated in the leaky fish. (**C**) Mosaic *spock1* crispants display increased leakage of the transgenic DBP-EGFP tracer outside of the vasculature (outlined by white dashed lines). (**D-E**) Dorsal view of whole mount HCR in situ for *spock1* (white) reveals expression throughout the brain of uninjected controls (D) but not in *spock1* crispants (E). (**F-G**) While controls confine the DBP-EGFP tracer (green) within the blood vessels (magenta) in the brain (F), *spock1* crispants display increased leakage into the brain parenchyma (G, outlined by white dashed line), corresponding with the loss of *spock1* expression (E). Scale bars represent 50 μm.
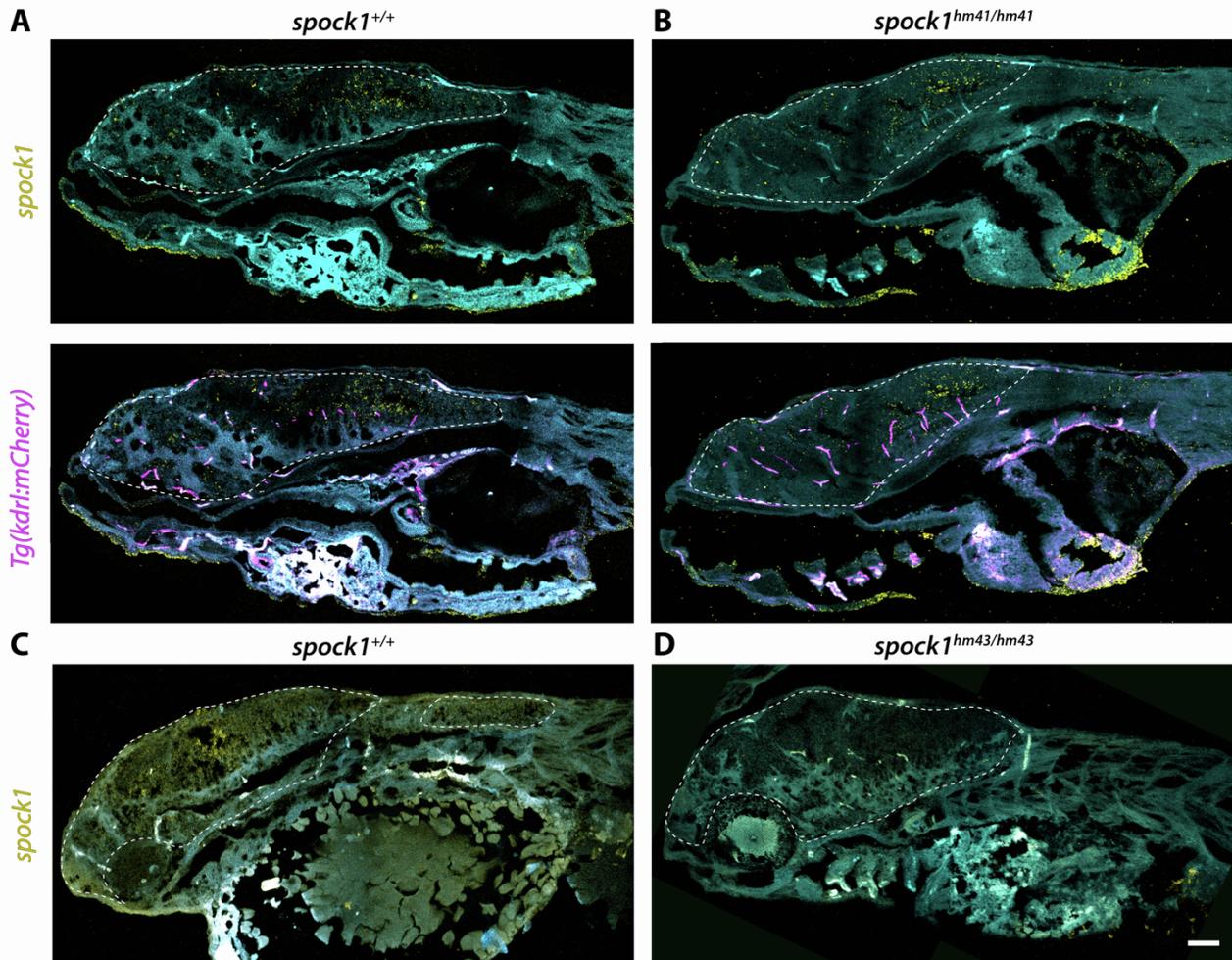
Figure S4. Expression of *spock1* is unaltered in *spock1^{hm41/hm41}* mutants and absent in *spock1^{hm43/hm43}* mutants, related to Figure 1. (**A-B**) *Spock1* expression (yellow) is found throughout the brain and spinal cord (outlined by a white dashed line) in wild type (A) and *spock1^{hm41/hm41}* mutant fish (B) at 5 dpf. *Spock1* expression never colocalizes with vascular *Tg(kdrl:mCherry)* expression (magenta). Tissue autofluorescence is depicted in turquoise. (**C-D**) Unlike *spock1^{hm41/hm41}* fish and wild type fish (C), *spock1^{hm43/hm43}* mutants, which completely lack the 5' UTR and start codon of *spock1*, do not have any detectable *spock1* expression (yellow) in the brain (D). Tissue autofluorescence is depicted in turquoise. The remaining signal in the yolk and blood vessels is due to tissue autofluorescence. Scale bar represents 50 μm.
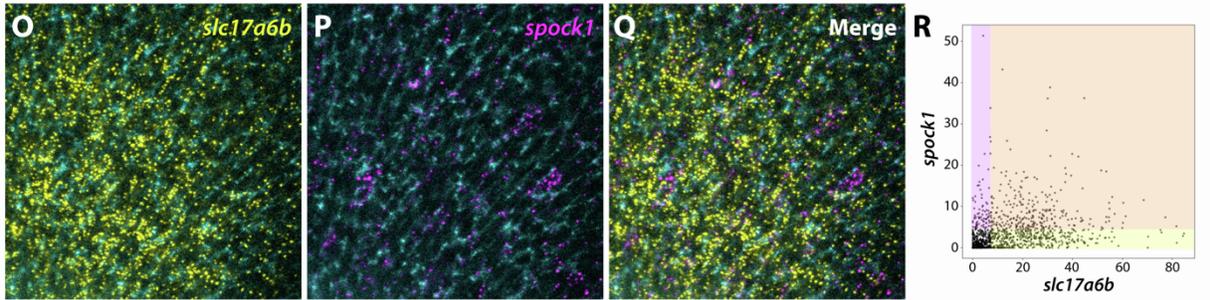
A TgKI(spock1:mCherry) **B** Tg(elavl3:GCaMP6s) **C** Merge

D TgKI(spock1:mCherry) **E** Tg(-3.1neurog1:GFP) **F** Merge

G Tg(actb2:memCitrine) **H** Segmented Cells **I** elavl3 spock1 **J**

K elavl3 **L** spock1 **M** Merge **N**

O slc17a6b **P** spock1 **Q** Merge **R**

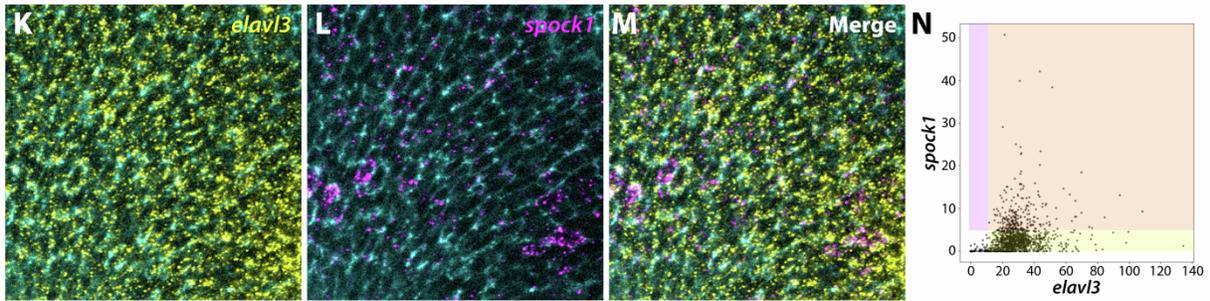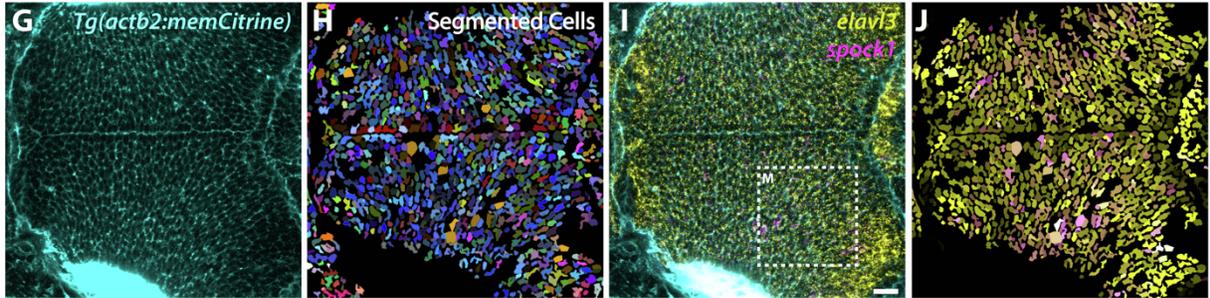**S** gad1b **T** spock1 **U** Merge **V**
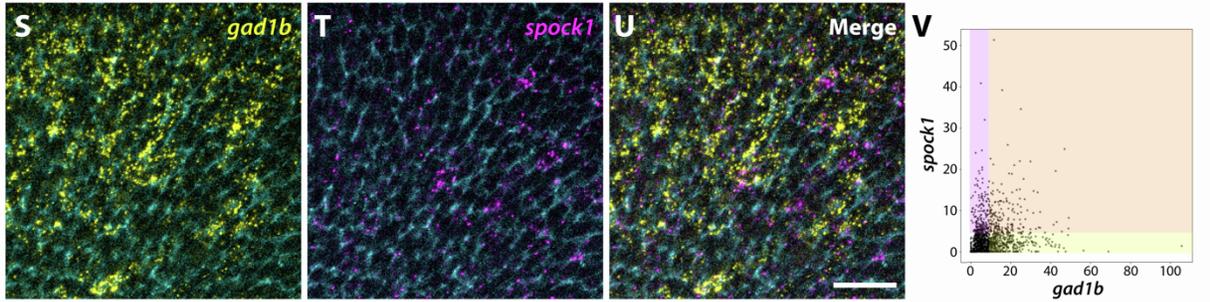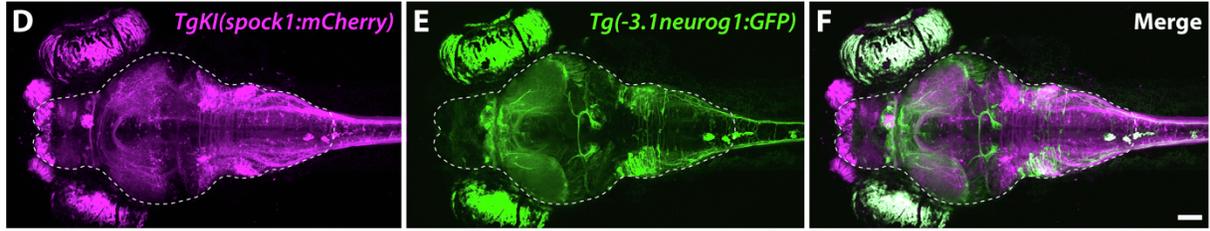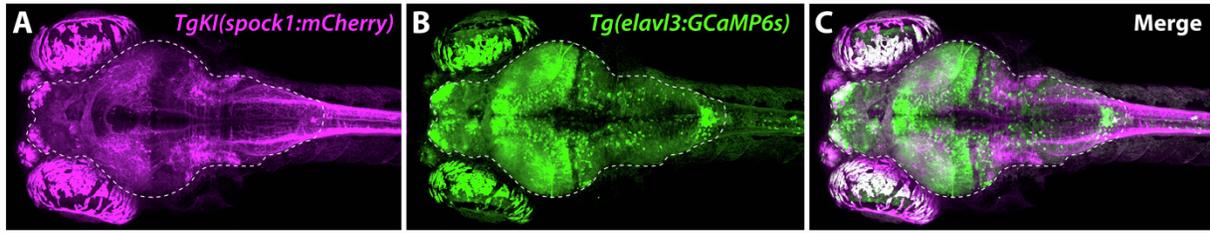
Figure S5. *Spock1* is expressed by a subset of post-mitotic neurons, related to Figure 2.
(**A-C**) *Spock1* expression (A, magenta) is found in a subset of active *elavl3+* postmitotic neurons
(B, green) throughout the 5 dpf brain (outlined by white dashed line). Iridophore pigment cells in
the eyes are autofluorescent in both channels, and not indicative of *spock1* expression. (**D-F**)
Spock1 (D, magenta) is not highly expressed by actively dividing *neurog1+* neurons (E, green) in
the 5 dpf brain (outlined by white dashed line). (**G-J**) Workflow of segmentation and quantification
of *spock1* co-expression with other neuronal genes. Using *Tg(actb2:mem-Citrine)* membrane-
labelled fish (G), we segmented individual cells in the brain (H), and then quantified expression
levels of *spock1* (magenta) and other neuronal markers, like *elavl3* (I-J, yellow) throughout the
entire midbrain. Boxed region in I marks region of brain used for zoom ins (M). (**K-N**) All *spock1*
(L) expressing cells were co-expressing the post-mitotic neural marker *elavl3* (K-N). (**O-R**) Some
glutamatergic neurons (O), marked by *slc17a6b* expression, express *spock1* (P-R). (**S-V**) Some
GABAergic neurons (S), marked by *gad1b* expression, express *spock1* (T-V). Scale bars
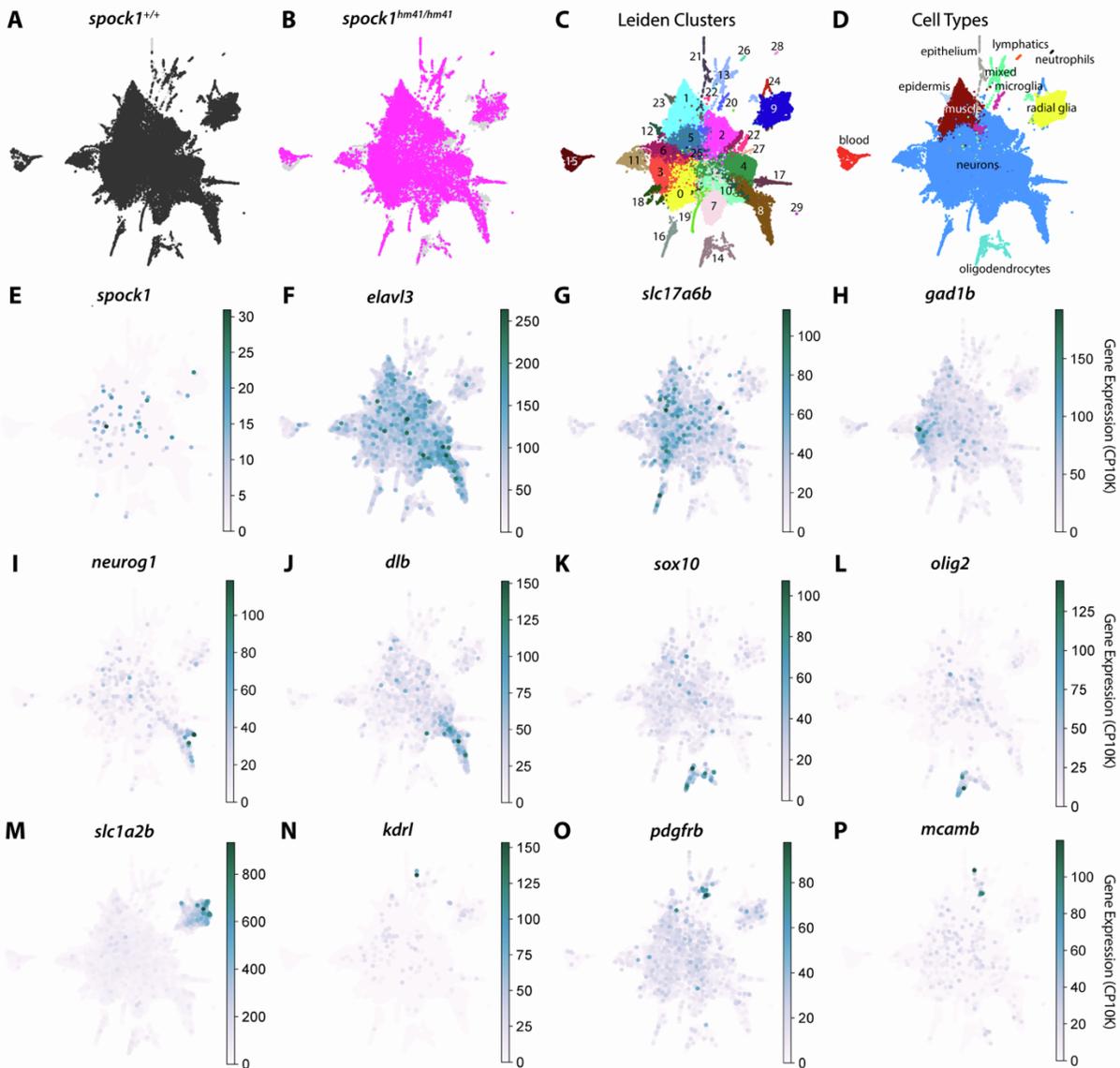represent 50 µm (F) and 20 µm (U).

Figure S6. scRNA-seq captures all neurovascular cells in both mutant and wild type larvae, related to Figure 6. (**A-B**) UMAP of the whole brain dataset shows overlap between wild type (A) and *spock1^{hm41/hm41}* mutant (B) cell type coverage, indicating that no cell type is absent in the mutant background. (**C**) UMAP with individual Leiden clusters annotated by color. (**D**) UMAP of the total data set separated by annotated cell type, with the vast majority of sequenced cells being neuronal (blue). Our data does capture blood cells (red), microglia (magenta), oligodendrocytes (aqua), radial glia (yellow), and other cells. (**E-P**) Gene expression plots for *spock1* (E), *elavl3* (F) marking postmitotic neurons, *slc17a6b* (G) for glutamatergic neurons, *gad1b* (H) for GABAergic neurons, *neurog1* (I) and *dlb* (J) for dividing neurons, *sox10* (K) and *olig2* (L) for oligodendrocytes, *slc1a2b* (M) for radial glia, *kdrl* (N) for vascular endothelial cells, *pdgfrb* (O) for pericytes and neurons, and *mcamb* (P) marking both endothelial cells and pericytes. These gene expression

plots reveal that *spock1* (E) is primarily expressed by postmitotic neurons and absent from the vascular cells (N-P).
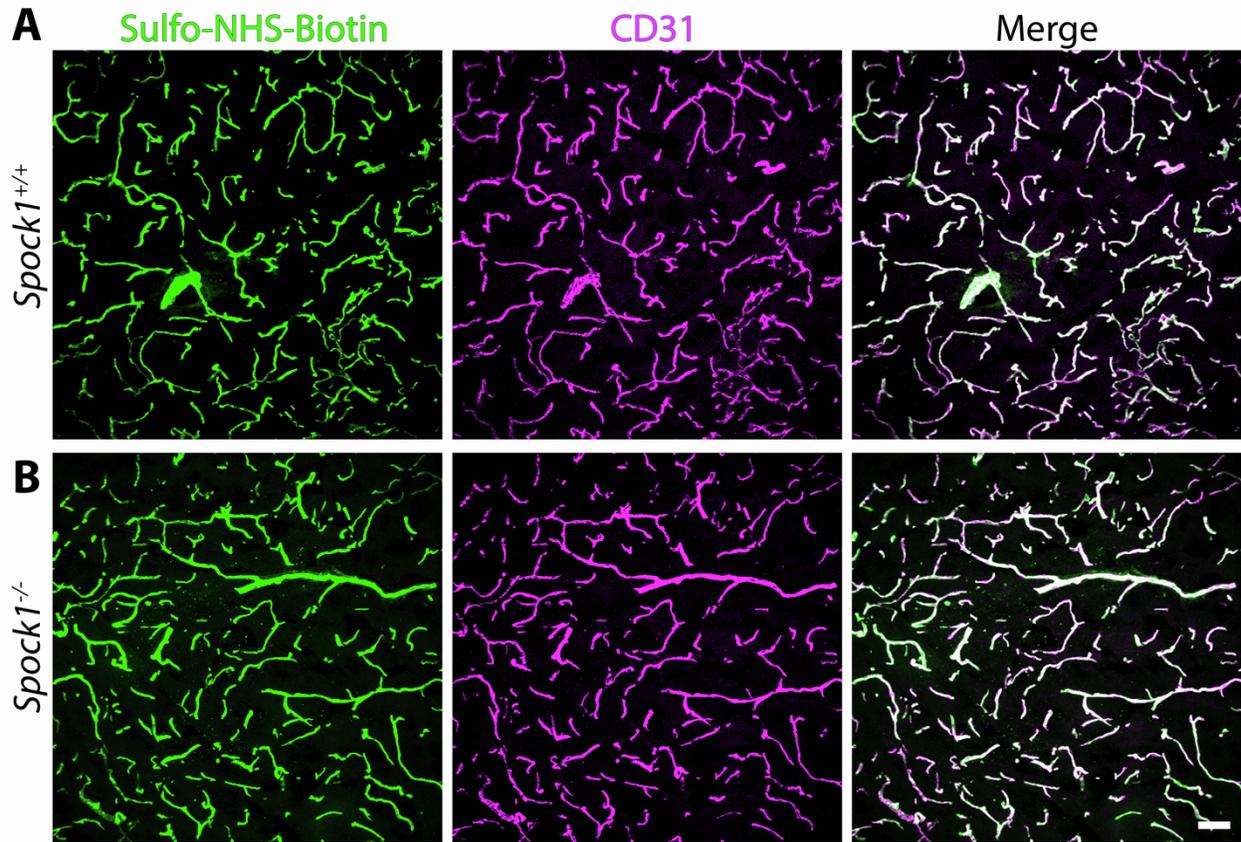
Figure S7. Adult *Spock1*^{-/-} mice recover BBB function, related to Figure 5. (**A-B**) Tracer leakage assays in adult wild type (A) and *Spock1*^{-/-} knockout mice (B) reveals that both genotypes confine the injected Sulfo-NHS-Biotin tracer (green) within the CD31+ vasculature (magenta), indicating a functional BBB. Scale bar represents 50 μm.